Proposal to JLab PAC43 May 18 2015

A study of the ΛN interaction through the high precision spectroscopy of Λ-hypernuclei with electron beam

JLab Hypernuclear Collaboration

Spokespersons:

F. Garibaldi[1], P.E.C. Markowitz[2], S.N. Nakamura[3], J.Reinhold[2], L. Tang[4,5], G.M. Urciuoli[1]

[1]*Istituto Nazionale di Fisica Nucleare, Sezione di Roma, Gr. Coll. Sanita',Viale Regina Elena 299, Rome, Italy*
[2]*Florida International University, Miami, Florida 33199, USA*
[3]*Department of Physics, Graduate School of Science, Tohoku University, Sendai, 980-8578, Japan*
[4]*Thomas Jefferson National Accelerator Facility, Newport News, Virginia 23606, USA*
[5]*Department of Physics, Hampton University, Hampton, Virginia, 23668, USA*

JLab Hypernuclear Collaboration

D. Lonardoni, A. Lovato
Argonne National Laboratory

D.J. Millener
Brookhaven National Laboratory

P.E.C. Markowitz (spokesperson), J.Reinhold (spokesperson)
Florida International University

G. De Cataldo, R. De Leo, D. Di Bari, L Lagamba, E. Nappi
INFN/Bari

E. Bellini, A. Giusa, V. Kuznetsov, F. Mammoliti, C. Potenza, G. Russo, H.J. Schulze
L. Sperduto, C. Sutera
INFN/Catania

L. Barion, G. Ciullo, M. Contalbrigo, E. Cravchenko, P.F. Dalpiaz, P. Lenisa, A. Movsisyan,
L.L. Pappalardo, F. Spizzo
INFN/Ferrara

M. Aghasyan, P.S. Anefalos, A. Courtoy, D. Hasch, M. Hoek, V. Lucherini, M. Mirazita,
R. Montgomery, J. Philips, S. Pisano, M. Turisini
INFN/Frascati

M.D. Anderson, M. Battaglieri, A. Celentano, R. De Vita, S. Fegan, M. Osipenko, M. Ripani,
M. Taiuti
INFN/Genova

R. Perrino
INFN/Lecce

E. Basile, O. Benhar, M. Capogni, E. Cisbani, S. Frullani, F. Garibaldi (spokesperson), F. Meddi, G.M. Urciuoli (spokesperson)
INFN / Rome

A. D'Angelo, C. Schaerf, M.L. Terranova, I. Zonta
INFN / Rome Tor Vergata

M. Agnello, E. Botta, S. Bufalino, A. Feliciello
INFN/Torino

P. Gueye, L. Tang (spokesperson)
Physics Department, Hampton University

T. Takahashi, Y. Sato
Institute for Particle and Nuclear Physics, KEK

T.Gogami
Division of Physics and Astronomy, Kyoto University

S. Gandolfi
Theoretical Division, Los Alamos national Laboratory

J. Pochodzalla, P.Achenbach
Institute fur KernPhysik, Johannes Gutenberg University Mainz

A.Ahmidouch
North Carolina A&T State University

C. Keppel, S.A. Wood
Thomas Jefferson National Accelerator Facility

S. Danagoulian,
Department of Physics, North Carolina A&T State University

E. Hiyama, M. Isaka
RIKEN

P. Bydžovský
Nuclear Physics Institute, Řež near Prague

T.Motoba
Laboratory of Physics, Osaka Electro-Communication University

V. M. Rodriguez
Universidad Metropolitana, San Juan, Puerto Rico

C. Samanta
Saha Institute of Nuclear Physics, & Virginia Commonwealth University

D. Lonardoni, F. Pederiva
Department of Physics, University of Trento and INFN gr. Collegato Trento

Y. Fujii, M.Fujita, M. Kaneta, H. Kanda, K. Maeda, S. Nagao,
S.N. Nakamura (spokesperson), Y.Takahashi, S. Tomita, Y.Toyama
Department of Physics, Graduate School of Science, Tohoku University

F.Pederiva
Physics Department, University of Trento and INFN-TIFPA

S.Kato
Department of physics, Yamagata University

J. Hoskins
College of William and Mary

A. Margaryan
Yerevan Physics Institute, Yerevan, Armenia

D. Androic
Department of Physics, University of Zagreb

T. Petkovic
Faculty of Electrical Engineering and Computing, Department of Applied Physics, University of Zagreb

Abstract

An ambitious and challenging experimental program was started at Jefferson Lab 15 years ago, producing high-resolution hypernuclear spectroscopy via the $(e, e'K^+)$ reaction. Data have been taken in both Hall A and Hall C on p-shell and medium-mass targets, providing clear spectra with 0.5~0.8-MeV energy resolution. The $(e, e'K^+)$ reaction spectroscopy of hypernuclei was established at JLab and it is now widely recognized as a powerful tool to study hypernuclei like (K^-,π^-) and (π^+, K^+) reactions. The $(e, e'K^+)$ reaction has advantages in energy resolution over hadronic probes and complements them in being a dominantly spin-flip reaction as opposed to a non-spin flip reaction. The greater strength observed for the low-lying excited states of $^{12}_{\Lambda}$B relative to the ground state is an example of the advantage sometimes afforded by the spin-flip capability. Gamma-ray spectroscopy, while extremely powerful, is limited to particle-bound states (and thus in light nuclei) and is able to measure level spacing. The $(e, e'K^+)$ reaction enables the determination of binding energies with high precision because of the calibration provided by the elementary reaction on hydrogen.

The elementary strangeness production process itself, fundamental to the interpretation of hypernuclear data, can be studied at forward angles where there is a lack of data and a wide disagreement among existing models. This proposal covers a coherent series of measurements on Λ hypernuclei in a wide mass range of targets to investigate the ΛN interaction and various forms of quantum-manybody systems. These measurements can be done only at JLab and are essential for theoretical investigations. The outcome will make significant contributions to hypernuclear physics research for the next decade(s) in the framework of the research either ongoing or planned in this field in the world. For this reason, since it is essential for further theoretical study of hypernuclei to collect enough information about Λ production on nucleons and about excitation spectra of a wide variety of Λ-hypernuclei, a continuation of the successful hypernuclear program at JLab is proposed. The new experimental design not only widens and deepens the physics range but also dramatically improves the data quality and production efficiency.

J-PARC has now re-started hypernuclear physics programs and the pion decay

spectroscopy technique has made great success at MAINZ. At GSI, a new exotic hypernucleus was claimed to be found. Even though plans for various new hypernuclear physics studies exist at different facilities, the precision, accurate mass spectroscopy of the JLab program has an unchallengeable position, in addition to the clearly known common advantages of electro-production (such as the size of momentum transfer, extra spin transfer from the virtual photon, converting a proton to a Λ for neutron rich hypernuclei *etc.*).

The 6 GeV experiments provided sufficient experience to establish the new program for CEBAF in the 12 GeV era. The outcome of the present activity is the base for building this experimental program, in the framework of the hypernuclear research that will take place in other laboratories with different, complementary techniques.

The new program represents an optimization that can broaden the physics investigation range and topics, and can also greatly improve production efficiency, maximizing the physics output dramatically.

1. Introduction

The major goal of nuclear physics is understanding the nature of strong interactions in hadronic many-body systems. In the universe, there is a hierachy of three such systems: 1) baryons/mesons, the bound system of quarks, 2) nuclei, the bound system of baryons and 3) neutron stars. The size scale of 1) and 2) is femtometers and that of 3) is ~10km. Though they differ by the order of 10^{19}, the interaction determining their structure and properties should be understood based on the same framework. The strong interaction in the low energy region where the QCD is not perturbative has been investigated in the framework of baryon potential models. Rich NN scattering experimental data provided quite precise nuclear-force models and detailed comparison between experimental studies of the nuclear structure and theoretical predictions indicated the importance of the 3-body force. Though the strange quark is heavier than the u, d quarks, it is still lighter than the QCD cut-off (~1GeV) unlike the masses of heavy quarks (c, t, b quarks) and the strange quark can be treated in the framework of the flavor SU(3) symmetry which is a natural extension of the isospin symmetry for ordinary nucleons. To create a unified description of the baryonic interaction within the flavor SU(3) basis, one must understand baryonic interactions beyond nucleon-nucleon (NN) interactions, such as hyperon-nucleon (YN) and hyperon-hyperon (YY) interactions. Spectroscopic investigation of Λ hypernuclei, a nuclear many-body system containing one Λ particle, provides a unique and currently the only practical tool to study the ΛN interaction, since direct ΛN scattering experiments are technically difficult.

Recent observation of ~2 solar mass neutron stars reveals that our understanding of the nuclear force with hyperons is not satisfactory though rich NN scattering data enabled us to construct precise NN interaction models.

It has been intensively discussed for the last decade that 3-body/4-body repulsive forces are necessary for the NN interaction to reproduce saturation while at the same time, the attractive NNN force is necessary to explain binding energies of A=3,4 nuclei. The density of the inner part of a neutron star is much higher than the normal nuclear density and thus hyperons appear naturally in order to reduce a nucleon's Fermi energy. However, inclusion of hyperons make the equation of state (EOS) too soft and thus 2 solar mass neutron star should not exist. Though there exist many discussion about the origin, the existence of such 3/4-body forces is naturally expected for the YN forces and the inclusion of such a force is one of solutions for the hyperon puzzle since such effects make the EOS hard enough to

support 2 solar mass neutron stars even with hyperons inside. It is expected that such 3/4-body YN forces make systematic shifts to the energy levels of medium to heavy hypernuclei at the few 100 keV level, which affects calculated maximum neutron star mass by ~30%. Therefore, precise Λ binding energy measurements of hypernuclei should be determined in medium to heavy hypernuclei. So far, heavier hypernuclear spectroscopy measurements were carried out with pion beams and both accuracy and precision are not sufficient. The absolute binding energies of all (π^+, K^+) hypernuclear data are based on the 6 events of $^{12}_{\Lambda}$C emulsion data while it is a very different case for the (e,e'K^+) experiments which can calibrate the absolute energy scales by the p(e,e'K^+)Λ/Σ^0 reactions. Recent precise hypernuclear data on $^{12}_{\Lambda}$B and $^{16}_{\Lambda}$N at JLab combined with careful re-examination of the consistency between emulsion data imply a possible half MeV shift of the $^{12}_{\Lambda}$C ground state energy which has a great impact on every measured hypernuclear binding energy using the (π^+, K^+) reactions. **Precise hypernuclear spectroscopy on medium to heavy hypernuclei with electron beams is only possible with the CEBAF electron beam and thus it is crucially important to obtain the reliable interaction which can be used to calculate EOS of the neutron stars.** It cannot be done at Mainz due to equipment constraints.

For the spectroscopy of light hypernuclei, the ΛN interaction can be studied more directly. Recent binding energy measurement of the $^{7}_{\Lambda}$He ground state at JLab triggered active discussion on the charge symmetry breaking (CSB) of the ΛN interaction. It is known that Λ binding energy differences of the ground states of A=4 hypernuclear iso-doublet ($^{4}_{\Lambda}$H and $^{4}_{\Lambda}$ He) are as large as 350 keV which is significantly larger than the effect of the Coulomb interaction (<50 keV) . Furthermore, it is much larger than the CSB effect for normal nuclei (binding energy difference between ^{3}H and ^{3}He is mostly determined by the Coulomb effect and only 70 keV originates from the CSB of the nuclear force). The origin of the ΛN CSB is discussed based on $\Lambda N - \Sigma N$ coupling effect (effective YNN 3-body force), but quantitative understanding of A=4 hypernuclear levels ($^{4}_{\Lambda}$H and $^{4}_{\Lambda}$ He, gs and 1st excited states) is not yet achieved. The mass difference between $^{4}_{\Lambda}$H and $^{4}_{\Lambda}$He ground states was phenomenologically introduced in the potential models. Recent progress of theoretical calculations enabled us to predict binding energies of the A=7 hypernuclear iso-triplet ($^{7}_{\Lambda}$He, $^{7}_{\Lambda}$Li*, $^{7}_{\Lambda}$Be). Except for $^{7}_{\Lambda}$He, the experimental values for binding energies were already obtained, but statistically limited emulsion data on $^{7}_{\Lambda}$He did not allow us to discuss the binding energy of this hypernucleus. The precise hypernuclear spectroscopy of $^{7}_{\Lambda}$He at

JLab provided a reliable binding energy and the comparison between experimental results on A=7 iso-triplet and theoretical results reveals that the CSB which is necessary for A=4 iso-double is not necessary for A=7 system. As mentioned before the CSB of the ΛN potential is quite important for the discussion of 3-body forces and ΛΣ mixing, however the situation is puzzling. The importance of a re-study of $^{4}_{\Lambda}$H and $^{4}_{\Lambda}$He with a state-of-art experimental technique is recognized and a new experiment on the ground state energy of $^{4}_{\Lambda}$H by the decay pion spectroscopy of hyperfragment was proposed originally at JLab and successfully carried out at MAINZ. At J-PARC, a gamma-ray measurement on the energy difference between ground state and 1st excited state of $^{4}_{\Lambda}$He is going to start. The needed information about the 1st excited state of $^{4}_{\Lambda}$H can be carried out only by the (e,e'K^{+}) spectroscopy at JLab. **With the combined information from such new experiments, the puzzle of the ΛN CSB effect will be clarified.**

In addition for light hypernuclear systems, recently striking news was reported from GSI, that a candidate of the nnΛ ($^{3}_{\Lambda}$n) system was observed [RAP13]. Existince of such an exotic state, a chargeless hypernucleus, contradicts the current understanding of the YN/NN interaction. The lightest hypernucleus whose existence is confirmed is $^{3}_{\Lambda}$H, but it is barely bound and its lifetime was recently put in question by the results of heavy ion experiments. Our understanding on the simplest system with hyperon may not be satisfactory and thus a systematic study is mandatory. **Only the (e, e′K^{+}) spectroscopy with both tritium and ^{3}He targets can give clear information about $^{3}_{\Lambda}$n and $^{3}_{\Lambda}$H.**

A truly comprehensive study of the role of hyperons should include light, medium mass and heavy nuclei. The few-nucleon systems are best suited to investigate the nature of three-body forces involving hyperons and nucleons, whereas medium size systems will provide valuable information on the level spectrum of the Λ. Finally, to address the long standing issue of the softening of the equation of state associated with the appearance of hyperons in compact stars, one must extend the analysis to the heaviest achievable nuclei, such as lead, the interior of which can approximately be described in terms of uniform nuclear matter.

[RAP13] C.Rappold *et al.*, *Phys. Rev.* C 88 (2013) 041001(R).

2. Proposed experiment

The proposed experiment aims to study the ΛN interaction through the precise spectroscopy of selected Λ hypernuclei. To achieve the above goal, we will take two experimental approaches: 1) study of light hypernuclear systems which are relatively simple and provide direct information about the ΛN interaction, and 2) systematic measurement of Λ binding energies (B_Λ) in medium to heavy hypernuclei in order to extend our knowledge to nuclear/hyperon matter to solve the hyperon puzzle which is one of the central issues in nuclear physics after the finding of two solar mass neutron stars.

All data obtained by the above two approaches are valuable to constrain the ΛN potential, however, lighter systems are suitable for extracting information about the charge symmetry breaking (CSB) effects by comparison with precise few-body calculations while heavier systems are useful to discuss the general tendency which is important for obtaining the equation of state (EOS) of neutron/hyperon stars.

The technique of $(e, e'K^+)$ hypernuclear spectroscopy is currently the only method which can measure the absolute hypernuclear mass centroids with an unprecedented accuracy of <100 keV. It should be noted that reaction spectroscopy such as $(e, e'K^+)$ hypernuclear spectroscopy provides information on the production cross sections as well as this binding energy information. The production information is complementary to the information obtained by decay product studies such as gamma and decay-pion spectroscopies.

In this section, the physics justification of individual measurements will be detailed.

2.1 Study of light hypernuclear systems

In order to solve the existing issues on the ΛN interaction, gaseous cryogenic hydrogen and helium targets will be used.

a) Elementary process of Λ electro-production

The $^1H\,(e, e'K^+)\Lambda, \Sigma^0$ reaction is the fundamental process to analyze data on electro-produced hypernuclei and furthermore experimentally it is **one of the key measurements to obtain an absolute missing mass calibration from the known Λ, Σ^0 masses**. The absolute mass calibration with a proton target is one of great advantage of the $(e, e'K^+)$ hypernuclear spectroscopy over meson induced reaction spectroscopy. Due to the lack of a neutron target, (π^+,K^+) and (K^-,π^-) spectroscopies need an energy scale reference

from other experiments.

The calibration of the energy scale is the primary objective of this measurement. However, study of the elementary reaction itself is also interesting in this kinematics region.

Though the small angle behavior of the electro-strangeness production is important to analyze electro-produced hypernuclear data, knowledge of the elementary cross section is far from satisfactory (see Figure 2-1). CLAS, SAPHIR and LEPS provided accurate photo-production data, however, they have difficulty reaching angles smaller than ~20^{o}.

Hypernuclear experiments at JLab (E94-107, E05-115) gave forward angle data, but the results are not consistent and their errors are large although kinematical conditions were not exactly same.

The photo- and electro-production of kaon-hyperon pairs on nucleons in the resonance region can be described by the isobar [DAV96,JAN01,MAR99] and Regge-plus-resonance [COR06] models. They predict different behaviors due to a lack of constraint from data at small angles. The proposing experiment will cover the range around $\theta_{\gamma K} \approx 0°$.

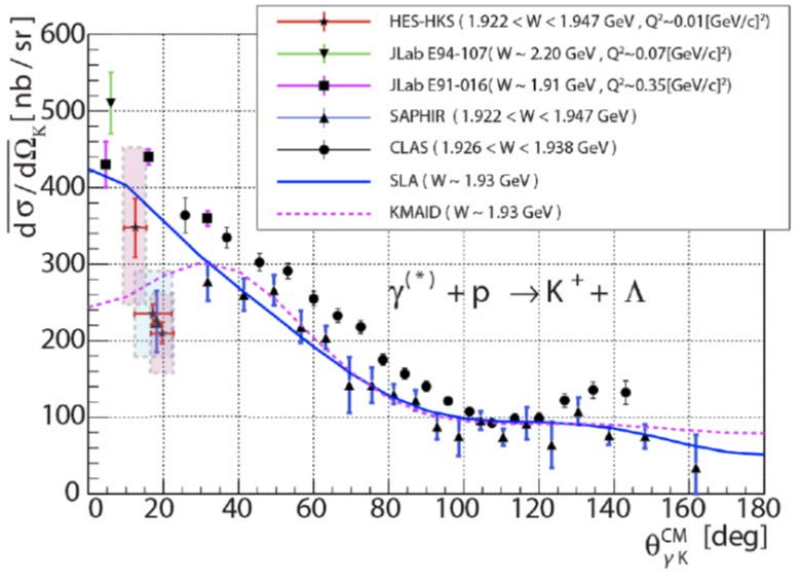

Figure 2-1: E94-107 electro-production result with Q^2 ~ 0.07 (GeV/c)^2, W=2.2 GeV and θ_{CM} =6^{o}, E05-115 (HKS-HES) with Q^2 ~ 0.01 (GeV/c)^2, W ~ 1.94 GeV and θ_{CM} ~ 15^{o} compared to photo-production data and models, all of them with W=2.2 GeV except for HKS-HES data. Error bar in E94-107 result represents total uncertainty (statistical and systematic uncertainties). HKS-HES data are separated in three angles and error bars show statistical and box systematic errors. CLAS data are from Ref. [BRA06] and SAPHIR data from [GLA04]. SLA [DAV96] and KMAID [MAR99] are isobar models' predictions.

Additionally the ratio of the $\Lambda:\Sigma^0$ final states will provide another constraint to the models. The isospin difference between the two final states leads to a simple prediction for the ratio of 3.7 in the quark model, although the isobar models have a range of predictions. The proposed measurement will show which model is correct.

[DAV96] J.C. David, C. Fayard, G.-H. Lamot, B. Saghai, *Phys. Rev.* **C 53**, 2613 (1996); T. Mizutani, C. Fayard, G.-H. Lamot, B. Saghai, *Phys. Rev.* **C 58**, 75 (1998).
[JAN01] S. Janssen, J. Ryckebusch, D. Debruyne, T. Van Cauteren, *Phys. Rev.* **C 65**, 015201 (2001).
[MAR99] T. Mart and C. Bennhold, *Phys. Rev.* **61**, 012201 (1999); C. Bennhold *et al.*,nucl-th/9901066.
[COR06] T. Corthals, J. Ryckebusch, and T. Van Cauteren, *Phys. Rev.* **C 73** (2006) 045207; T. Corthals, T. Van Cauteren, J. Ryckebusch, D.G. Ireland, *Phys. Rev.* **C 75** (2007) 045204; L. De Cruz, D.G. Ireland, P. Vancraeyveld, and J. Ryckebusch, *Phys. Lett.* **B694** (2010) 33; L. De Cruz, T. Vrancx, P. Vancraeyveld, and J. Ryckebusch, *Phys. Rev. Lett.* **108** (2012) 182002.
[BRA06] R. Bradford *et al.*, *Physical Review* **C 73**, 035202 (2006)
[GLA04] K. -H. Glander *et al.*, *Europian Physical Journal* **A 19**, 251 (2004); M. Q. Tran *et al.*, *Physical Letters* **B 445**, 20 (1998).

b) The ΛN interaction and charge-zero exotic hypernuclei ([nΛ], [nnΛ])

The study of s-shell hypernuclei is mostly motivated by the study of the ΛN interaction since precise few-body calculation techniques are well established and it enables us to study the ΛN interaction with less ambiguity. So far, it has been commonly believed that the lightest Λ-nucleus system is ${}^{3}_{\Lambda}$H. However, it recently was reported that an indication for a **chargeless Λ-nucleus [nΛ] or [nnΛ]** was observed at GSI [RAP13].

There are many experimental as well as theoretical reasons to believe that the [nΛ] system is not bound, but there is no experimental evidence that the [nnΛ] system is not bound. The experimental resolution and calibration tools of the GSI experiment were limited and thus it was not yet widely accepted that the observed system is the [nnΛ] bound system, which was never found in intensive studies using kaon beams in the 80's.

Obviously the momentum transfer in the heavy ion collision is higher than for the meson exchange reaction using a kaon beam. Since most of the theoretical models predict no [nΛ] and [nnΛ] bound states, confirmation of the existence or the non-existence of these systems should be experimentally clarified. **Clear finding of the [nnΛ] bound system means that our understanding of even the simplest hypernuclear system is imperfect and requires the existing theories to be updated.**

The (e, e′K) spectroscopy with hydrogen isotope targets is direct and the clearest way to test the existence of such a system. The ^{2}D(e, e′K^{+})[nΛ] and ^{3}T(e, e′K^{+})[nnΛ] reactions are sensitive to not only the bound systems but also resonance states.

Using the expected hypernuclear yield given in Table 4-II, 200 mm, 200 psi of gaseous deuterium (59 mg/cm^{2}) with 20μA beam will give 0.38 counts/h for a 1 nb/sr cross section. 130 hours of running will provide 5σ-sensitivity to the existence of narrow peak of 1 nb/sr or set an upper limit. It should be mentioned that the shape of the missing mass spectrum of quasi-free Λ production would provide precious information about the ΛN potential from the final state interaction so that the data (even with a negative result for the bound state) will provide useful information on the ΛN potential in addition to exploring the existence of [nΛ] bound system.

For the tritium target, a similar design for the cryogenic target cell to the JLab MARATHON experiment would be adopted. A gaseous target of 250 mm length, 200 psi will provide 89 mg/cm^{2} and determine either a 5σ-sensitivity on the existence of a narrow peak of 1 nb/sr or set an upper limit using 130 hours of beam time. By using ^{3}He gaseous target, the established lightest hypernuclei $^{3}_{\Lambda}$H can be produced. It will provide a calibration and reference for all gaseous target data taken in the proposed experiment.

[RAP13] C.Rappold *et al.*, *Phys. Rev.* **C 88** (2013) 041001(R).

c) Charge Symmetry Breaking (CSB) of the ΛN interaction

The s-shell hypernuclei ($^{3}_{\Lambda}$H, $^{4}_{\Lambda}$H, $^{4}_{\Lambda}$He, and $^{5}_{\Lambda}$He) provide a very important testing ground for the ΛN interaction. In particular, the hypertriton and the A = 4 hypernuclei can be treated exactly in Faddeev and Faddeev-Yakubovsky calculations [NOG02], respectively, and all can be treated by a variety of few-body techniques. It is known that the

binding energies of s-shell hypernuclei cannot be understood without inclusion of the coupling of the Λ and Σ channels via the NΛ-NΣ interaction that can be treated as an effective ΛNN three-body interaction illustrated in Fig. 2-2 [AKA10].

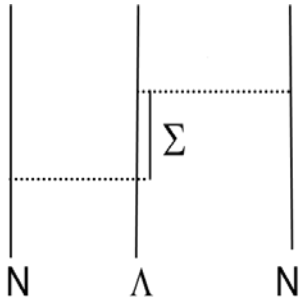

Figure 2-2: ΛΣ coupling in the ΛNN three-body force

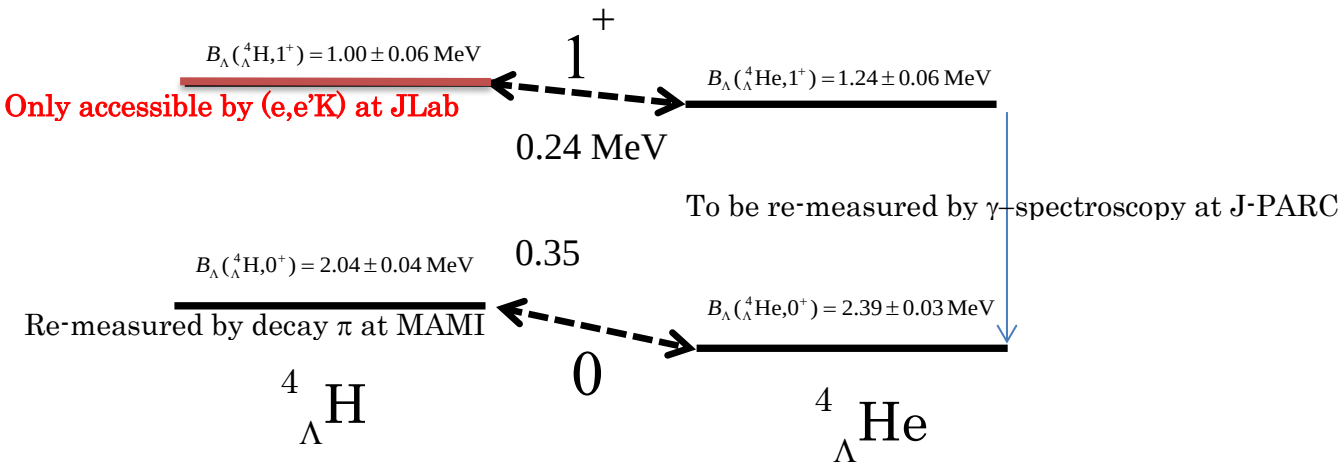

Figure 2-3: Energy levels for ground and 1st excited states of A=4 hypernuclear iso-doublet.

The ΛN-ΣN coupling selectively increases the binding energies of the 0^+ ground states of the A=4 hypernuclei and is thereby also responsible for about half of the spacing between the 1^+ and 0^+ states in Fig. 2-3. The remainder of the $1^+/0^+$ spacing is due the ΛN spin-spin interaction, because the singlet interaction is more attractive than the triplet interaction in s-waves. Substantial Σ admixtures are present because the Λ and Σ differ in mass by only 80 MeV and because one-pion exchange, absent for ΛN-ΛN, is important for ΛN-ΣN.

As shown in Fig. 2-3, the measured binding energies of the A = 4 hypernuclear iso-doublet's ground states differ by a few hundred keV. The difference caused by Coulomb effects is expected to be at the 50 keV level, and it is in the opposite direction needed to explain the measured binding energy difference. In the few-body calculations, the CSB is driven by the 8 MeV mass differences between the Σ^- and Σ^+ hyperons that form the main admixtures in ${}^4_\Lambda$H and ${}^4_\Lambda$He, respectively. However, **a consistent understanding of the 0^+ and 1^+ states of ${}^4_\Lambda$H and ${}^4_\Lambda$He has not yet been obtained**. Thus the ground-state binding energies in Fig. 2-3, which come from emulsion data [DAV05], and the 1^+ excitation energies that were obtained in low-statistics experiments with NaI detectors [BED83], need to be re-examined.

With emulsion results on ${}^7_\Lambda$Li and ${}^7_\Lambda$Be, and a recent measurement of ${}^7_\Lambda$He by the (e, e′K^+) reaction at JLab [NAK13], all the ground state energies of the A=7, T=1 hypernuclear iso-triplet (${}^7_\Lambda$He, ${}^7_\Lambda$Li* and ${}^7_\Lambda$Be) were experimentally obtained. They were compared to a four-body cluster calculation (αNNΛ) [HIY90] with and without inclusion of a phenomenological CSB potential which was introduced to reproduce Λ binding energy differences of the A=4 hypernuclear iso-doublet, ${}^4_\Lambda$H and ${}^4_\Lambda$He. Inclusion of the CSB potential which is necessary for the A=4 hypernuclei makes the agreement between the experimental results and the theoretical prediction worse for the A=7 hypernuclear iso-triplet.

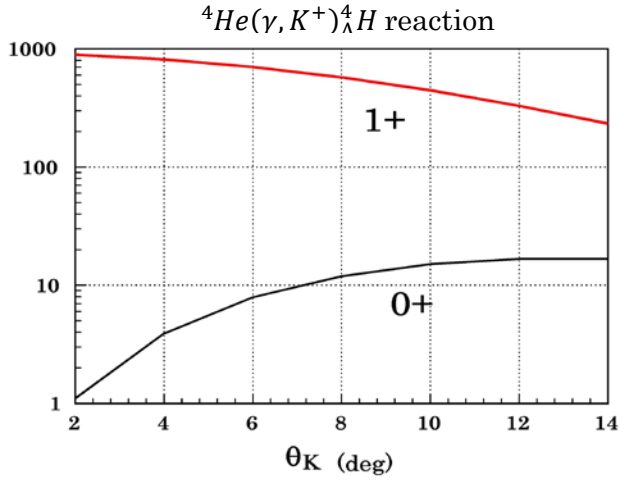

Figure 2-4: Expected cross sections for 0^+ and 1^+ states of ${}^4_\Lambda$H by the (e, e′K^+) reaction [MOT14].

This implies that the current phenomenological CSB potential is too naïve or the binding energies of $^{4}_{\Lambda}$H and $^{4}_{\Lambda}$He, which are the starting points of this discussion, need to be re-measured with the state-of-the-art experimental techniques. The excitation energy of $^{4}_{\Lambda}$He is going to be measured with a Ge-array (Hyperball) now at J-PARC, and the decay pion spectroscopy for $^{4}_{\Lambda}$H at MAMI-C determined the precise binding energy of the $^{4}_{\Lambda}$H ground state. **The proposed ^{4}He(e, e′K^{+})$^{4}_{\Lambda}$H* reaction measures the binding energies of the 1st excited level (1^{+}) which is only accessible by the (e, e′K^{+}) reaction.**

Although the excitation energy of the 1^{+} state of $^{4}_{\Lambda}$H is only ~1 MeV, the (e, e′K^{+}) reaction predominantly populates the 1^{+} state at forward angles due to the large spin-flip amplitude. The production cross section of the 1^{+} is expected to be more than 50 times larger than that of 0^{+} at $\theta_K < 8$ deg. [MOT14] (see Fig.2-4) and thus there is a negligible effect from the 0^{+} ground state on the spectrum to be measured by the proposed experiment.

Yield of the $^{4}_{\Lambda}$H ground state was estimated with the production cross section of $^{4}_{\Lambda}$H as taken from JLab E91-016 [DOH04] at ~20 nb/sr for forward $\theta_{\gamma K}$ angles in the photon-nucleus CM system where we assumed that all of the yield originated from the 1^{+} state. We scaled the counting rate for the elementary process from the $^{12}_{\Lambda}$B yield and normalized it to 58 mg/cm^{2} (20cm long, 200psi) of helium gas target with 20μA beam, to find that a counting rate of 3.8/h of $^{4}_{\Lambda}$H events can be expected.

In order to have 1000 events in the $^{4}_{\Lambda}$H 1^{+} state so that excitation energy is measured with a statistical error of 20 keV,

266 h = 11 days of beam time

is necessary.

[NOG02] A. Nogga, H. Kamada, and W. Glöckle, Phys. Rev. Lett. 88 (2002) 172501.
[AKA10] Y.Akaishi, *Prog. Theo. Phys. Suppl.* **186** (2010) 378.
[DAB05] D.H. Davis, *Nucl. Phys.* **A 754** (2005) 3c.
[BED83] M. Bedjidian *et al., Phys. Lett.* **B 83** (1979) 252.
[NAK13] S.N.Nakamura *et al*. (HKS collaboration), *Phys.Rev. Lett.* **110** (2013) 012502.
[HIY09] E. Hiyama *et al., Phys. Rev.* **C 80** (2009) 054321.
[MOT14] T. Motoba, private communication.
[DOH04] F.Dohrmann *et al., Phys. Rev. Lett.* **93** (2004) 242501.

2.2 Systematic measurement of B_Λ for heavier hypernuclei

a) Objective of precise measurement of B_Λ for heavier hypernuclei

Neutron Stars and the Hyperon Puzzle

Neutron stars (NS) are the most compact and dense stars in the universe, with typical masses $M \sim 1.4\ M_\odot$ and radii R~10 km. Their central densities can be several times larger than the nuclear saturation density $\rho_0 = 0.16$ fm^{-3}. The Fermi energy of fermions at such densities is in excess of tens of MeV and hence thermal effects have little influence on the structure of NS. Therefore they exhibit the properties of cold matter at extremely high densities, very far from being realized in present terrestrial experiments. In the era of multi-messenger astronomical observations, NS offers a unique opportunity to test a broad class of theories, from nuclear physics to general relativity.

From the surface to the interior of a NS stellar matter undergoes a number of transitions. From electrons and neutron rich ions in the outer envelopes, the composition is calculated to change to a degenerate gas of neutrons, protons, electrons and muons in the outer core. At densities larger than ~$2\rho_0$ new hadronic degrees of freedom or exotic phases are likely to appear.

The first theoretical indication for the appearance of hyperons in the core of a NS was already advocated in 1960 [AMB60]. In the degenerate dense matter forming the inner core of a NS, Pauli blocking would prevent hyperons from decaying by limiting the phase space available to nucleons. When the nucleon chemical potential is large enough, the conversion of nucleons into hyperons becomes energetically favorable. This results in a reduction of the Fermi pressure exerted by the baryons and a softening of the equation of state (EOS). As a consequence, the maximum mass determined by the equilibrium condition between gravitational and nuclear forces is reduced. The value of about 1.4 $M_\odot$ for the maximum mass of a NS, inferred from neutron star mass determinations [THO99], was considered the canonical limit, and it was compatible with most EOS of matter containing strangeness. However, the recent measurements of the large mass values of the millisecond pulsars J1614-2230 (1.97(4) $M_\odot$) [DEM10] and PSR J0348+0432 (2.01(4) $M_\odot$) [ANT13] require a much stiffer equation of state.

This seems to contradict the appearance of strange baryons in high-density matter given what is known at present about the hyperon-nucleon interaction. This apparent inconsistency between NS mass observations and theoretical calculations is a long standing

problem known as **hyperon puzzle**. Its solution requires better understanding of the YN interaction in a wide range of systems from light to medium and heavy hypernuclei as well as more accurate theoretical calculation frameworks.

Currently there is no general agreement (even qualitative) among the predicted results for the EOS and the maximum mass of NS including hyperons. This has to be ascribed to the combination of an incomplete knowledge of the forces governing the system (in the hypernuclear case both two- and three-body forces), and to the concurrent use of approximated theoretical many-body techniques.

The rich nucleon-nucleon scattering data allows us to derive satisfactory models of two-body nuclear forces (NN) and no scattering data exist in the YY sector. The main reasons of this lack of information lie in the short lifetime of hyperons in the vacuum and the difficulty of collecting YN and YY scattering data although a ΣN scattering experiment is currently in preparation at J-PARC [MIW11]. Therefore, the realistic YN interaction models use the measured binding energies of hypernuclei as constraints.

Similarly, in the non-strange nuclear sector the binding energies of light nuclei have been used to constrain three-nucleon potential models. However, the most accurate phenomenological three-body force (Illinois 7), while providing a satisfactory description of the spectrum of light nuclei up to ^{12}C [PIE08] yields to a pathological EOS for pure neutron matter (PNM) [MAR13]. On the other hand, when additional information on the three-nucleon interaction is inferred from saturation properties of symmetric nuclear matter (Urbana IX force), the resulting PNM EOS turns out to be compatible with astrophysical observations [GAN12].

Recent analysis of ^{16}O-^{16}O scattering data shows that the established meson exchange potential model (Nijmegen ESC08c) cannot reproduce the cross section for large scattering angles and inclusion of 3-body/4-body repulsive forces solves the problem [FUR09]. This is also an indication that 3-body/4-body repulsive forces become more significant at higher density.

In a similar fashion, the binding energies of light hypernuclei do not suffice in constraining hypernuclear interactions. Behavior of such repulsive forces at higher density can be studied more clearly in heavier hypernuclear system. Additional information must necessarily be inferred from the properties of medium and heavy hypernuclei in order to extrapolate to the infinite limit.

Theoretical efforts

So far, the structure of heavier Λ hypernuclei has been calculated based on the weak-coupling approximation that assumes the wave function of a Λ hypernucleus can be decomposed into a core nucleus and a Λ hyperon. In this framework, the hypernuclear Hamiltonian consists of a Hamiltonian for the core-nucleus, the Λ kinetic energy and the sum of ΛN effective interactions that were derived from the free ΛN interaction by the G-matrix calculation. This approach worked quite successfully and the structure of heavier hypernuclei data mostly obtained by the (π^+,K^+) reaction with resolutions of a few MeV have been analyzed successfully.

Analysis of hypernuclear binding energies and a limited number of YN scattering data enabled the construct of reliable baryon-baryon interaction models based on meson exchange picture such as Nijmegen ESC08c. Recently, 3/4-body repulsive forces (MPa) were added to ESC08c which worked fine at the normal nuclear density but could not explain the ^{16}O-^{16}O scattering data at large scattering angles, *ie.* at larger density [FUR09]. The ESC08c+MPa were applied to calculate Λ binding energies of hypernuclei (Fig. 2.5 (a)) and neutron star's mass as a function of radii [YAM14].

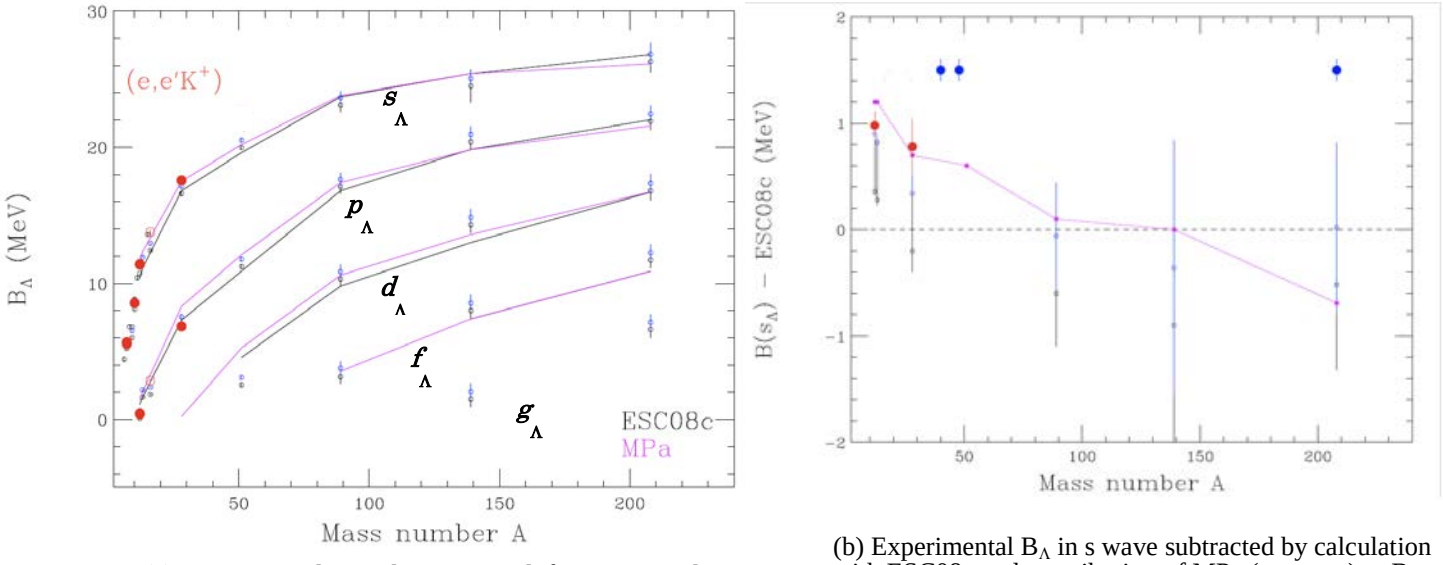

(a) Experimental B_Λ values in s, p, d, f, g waves and calculation results with ESC08c (black) and ESC08c + MPa (magenta). Data for A>50 were obtained from the (π^+,K^+) hypernuclear spectroscopy.

(b) Experimental B_Λ in s wave subtracted by calculation with ESC08c and contribution of MPa (magenta) to B_Λ. Blue points with error bars show the expected accuracy of the proposed experiment.

Figure 2-5: Λ separation energies as a function of A.

As already mentioned, the experimental B_Λ in medium to heavy hypernuclei were mostly obtained by the (π^+,K^+) reactions. Fig. 2-5 (b) shows the residuals of such experimental values and the ESC08c + MPa calculation after a subtraction of that with only ESC08c to examine the contribution from 3/4- body forces. It shows a systematic dependence on mass number A, but the existing experimental data from the (π^+,K^+) hypernuclear spectroscopy with about 1 MeV level of precision are not accurate enough to discuss such a small 3/4-body effects. It should be noted that the B_Λ in p, d, f, g waves in hypernuclei are sensitive to different densities and thus additional constraints to theories can be obtained.

Though 3/4-body forces give a small effect on the B_Λ at around the normal nuclear density, it will give a significant effect at higher densities and make the nuclear EOS hard enough to support 2 solar mass neutron stars as illustrated by Fig.2-6.

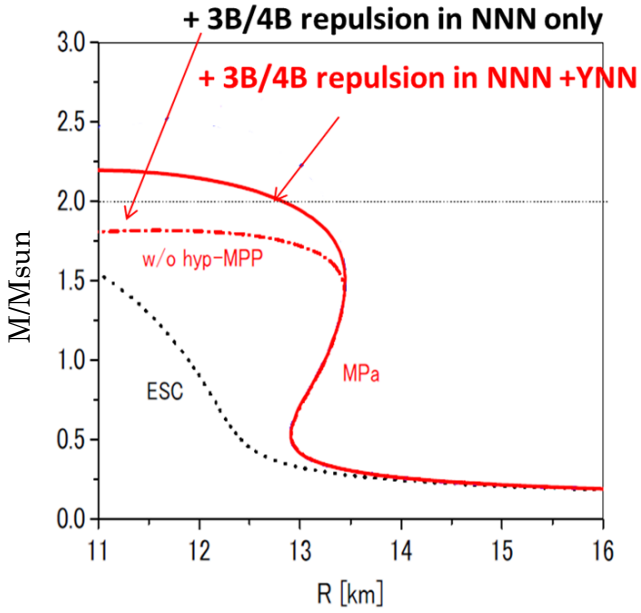

Figure 2-6: Calculated neutron star mass as a function of radii [YAM14]. The result with only Nijmegen ESC08c makes EOS too soft (dots), but inclusion of 3/4 body repulsion force in nucleon sector makes it harder (dot-line) and inclusion of it in hyperon sector as well as normal sector solve the hyperon puzzle (solid).

The G-matrix calculation based on the meson exchange potential is not the only study to relate hypernuclear data to neutron stars. Recently, a different calculational approach using a mean field calculation such as Auxiliary Field Diffusion Monte Carlo (AFDMC) has made great progress. An accurate calculation of the Λ separation energy B_Λ of light- and medium-heavy hypernuclei by AFDMC has been carried out [LON14] using a

phenomenological interaction [BOD84,USM95,IMR14] in which the two-body part was fit to the existing Λp scattering data. As shown in Fig. 2-7(a), when only the two-body ΛN force is considered (red curve), the calculated hyperon separation energies tend to disagree with the experimental data (green curve) as the density increases. Inclusion of the 3-body ΛNN force in this scheme leads to a satisfactory description of the hyperon separation energies in a much broader mass range and for the Λ occupying different single particle state orbitals (s, p and d wave), as shown in Fig. 2-7(b).

However, potential models predicting relatively small differences in the Λ separation energies of hypernuclei give dramatically different results for the properties of an infinite medium [YAM14,LON15]. The resulting EOS spans all the regimes from the appearance of a substantial fraction of hyperons at ~$2\rho_0 \simeq 0.32$ fm^{-3} to the absence of Λ particles in the whole density range of the star (Fig. 2-8(a)). This has a sizable effect on the prediction of the NS structure (Fig. 2-8(b)) which shows understanding of the 3-body force is a key to solve the hyperon puzzle as Fig. 2-6 by the G-matrix calculation shows.

Therefore, the derivation of realistic hypernuclear potential models is of paramount importance to properly assess the role of hyperons in NS and reconcile theoretical predictions with astrophysical observations. This demands new experimental investigation with improved precision on the hypernuclear properties for at least two species in the medium to heavy mass region. In order to meet the requirement, we propose B_Λ measurements of hypernuclei in A=40-50 and A=208 with a centroid accuracy of 100 keV.

b) Spectroscopy for A=40-50 hypernuclei

The region of medium-mass hypernuclei is particularly interesting. Systems with $A \leq 50$ are the most similar to the infinite medium for which ab-initio many-body calculations are feasible. However, present experimental information in the mass region $40 \leq A \leq 50$ relies uniquely on the data measured by the (π^+, K^+) reaction. The resolution as well as absolute energy scale calibration of the (π^+, K^+) data must be improved. The only two hypernuclei for which experimental data exist are ^{40}Ca [PIL91] and ^{51}V [HOT01], the former plagued by very low statistics (Fig. 2-9). Hence, new accurate (e, e'K^+) measurements of the Λ separation energies in the regions A~40 and A~50 are necessary to constrain the behavior of hypernuclear interactions at densities relevant for neutron star matter.

For instance, precise measurements of B_Λ in $^{40}Ca(e, e'K^+)_\Lambda{}^{40}K$ and $^{48}Ca(e, e'K^+)_\Lambda{}^{48}K$ could provide such data as well as assess the isospin dependence of the phenomenological three-body hyperon-nucleon force. However, experimental data suitable to establish a possible asymmetry between the Λnp and the Λnn interactions are rather scarce and affected by large uncertainties. The present parametrization of the ΛNN potential, based on a fit to symmetric hypernuclei, includes a contribution that can be written in terms of projectors on the triplet (T = 1) and singlet (T = 0) nucleon isospin channels. Introducing an additional parameter C_T, it is possible to gauge the strength and the sign of the Λnn contribution. Fig2-10 shows preliminary results for the Λ separation energies obtained by the AFDMC calculation varying C_T from -2 to 3. The B_Λ are normalized with respect to the $C_T = 1$ case for which the original three-body force is recovered. The grey bands represent the 2% and 5% variations of the ratio $B_\Lambda/B_\Lambda(C_T = 1)$.

For light hypernuclei the results are compatible with the measured B_Λ in the range of $-1 \leq C_T \leq 1.5$, which implies that the isospin asymmetry contribution is essentially undetermined. This is due the fact that the Pauli principle, particularly effective in symmetric systems, suppresses any strong contribution from the Λnn or Λpp channels. However, Fig.2-10 shows that asymmetric hypernuclei are more sensitive to the variation of C_T, in particular for $^{49}{}_\Lambda Ca$, the heaviest system which AFDMC has calculated in this mass region. Thus, precise $(e, e'K^+)$ measurements of the Λ separation energies of $^{40}Ca(e, e'K^+)^{40}_\Lambda K$ and $^{48}Ca(e, e'K^+)^{48}_\Lambda K$ will provide strong constraints on the value of C_T and thus on the three-body hyperon-nucleon interaction.

Establishing the isospin dependence of the ΛNN force is of major interest. In a quite asymmetric nucleus as $^{48}_\Lambda K$, where $\delta = (N - Z)/A \simeq 0.19$, the C_T dependence of B_Λ is appreciable due to the larger contribution arising from Λnn triplets. In NS matter the asymmetry parameter is $\delta \simeq 0.9$, and thus the role of the isospin asymmetry is crucial in the determination of the NS structure.

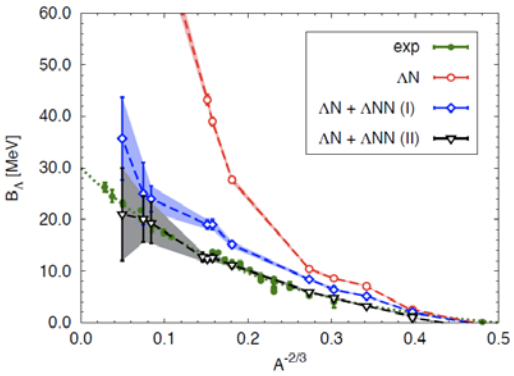

(a) Experimental B_Λ values in s wave and AFDMC calculation results with 2-body ΛN interaction alone, and two different parametrizations of the 3-body YN interaction

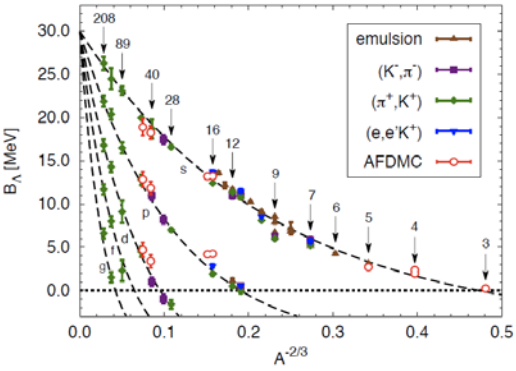

(b) Experimental results for Λ in s, p, d, f and g waves. Red empty dots are the AFDMC results obtained including the most recent 2-body plus 3-body hyperon-nucleon phenomenological interaction model.

Figure 2-7: Λ separation energies as a function of $A^{-2/3}$.

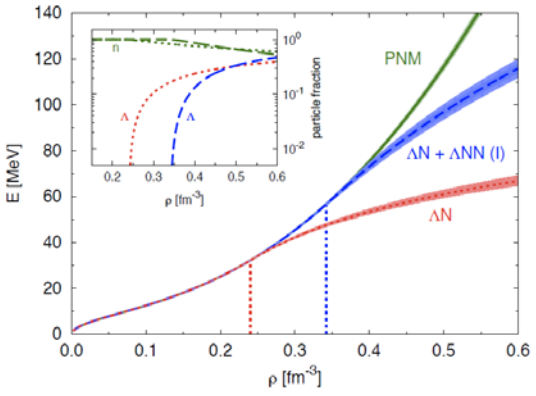

(a) Equations of state. The vertical dotted lines indicate the Λ threshold densities. In the inset, neutron and Λ fractions corresponding to the two hyper-neutron matter EOSs.

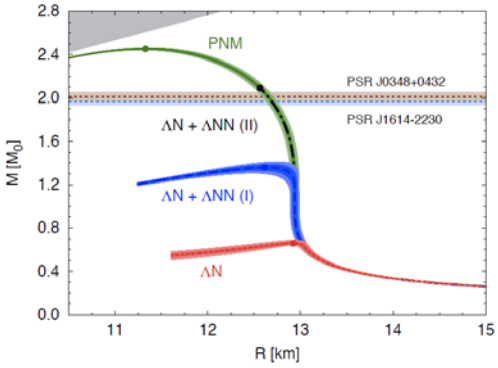

(b) Mass-radius relations given by AFDMC. Full dots represent the predicted maximum masses. Horizontal bands at $2M_\odot$ are the observed masses of the heavy neutron stars [DEM10,ANT13].

Figure 2-8: EOS and neutron star mass-radius relations calculated by AFDMC.

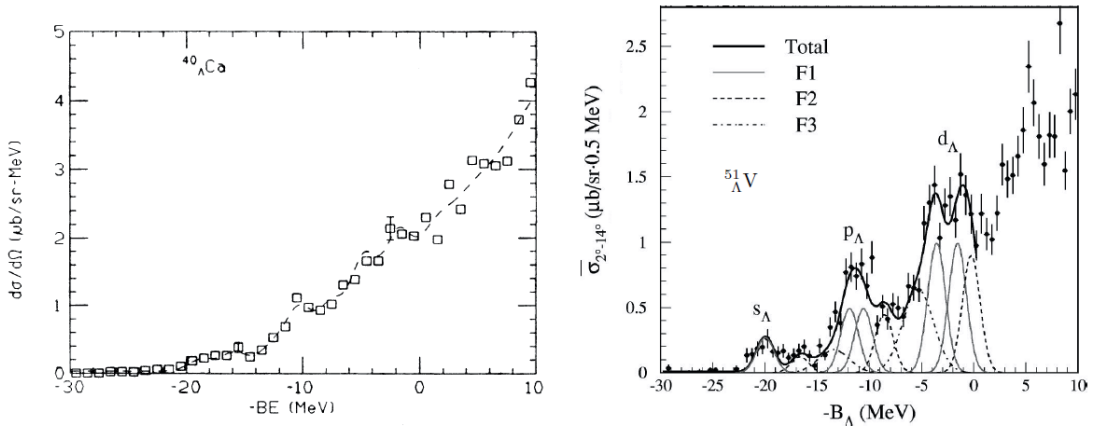

Figure 2-9: $^{40}_{\Lambda}$Ca [PIL91] and $^{51}_{\Lambda}$V [HOT01] spectra obtained by the (π,K) reaction.

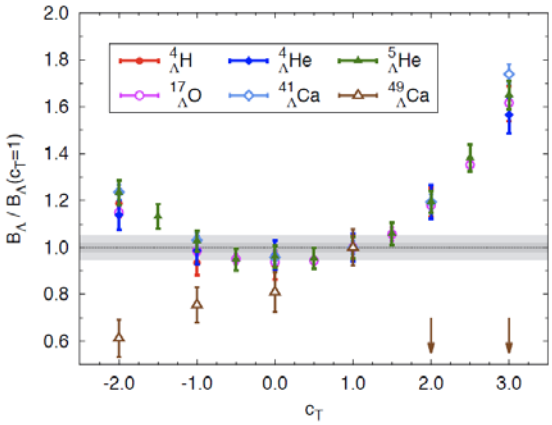

Figure 2-10: Λ separation energies normalized with respect to the C_T = 1 case as a function of C_T. Grey bands represent the 2% and 5% variations of the ratio B_Λ/B_Λ (C_T = 1). Brown vertical arrows indicate the results for ^{49}Ca in the case of C_T = 2 and C_T = 3, outside the scale of the plot.

c) Spectroscopy for A=208 hypernucleus

In view of its astrophysical implications, the extension of the proposed experiment to a heavy nuclear target, such as ^{208}Pb, in which the properties of a bound hyperon are likely to be little affected by surface effects, is of primary importance.

The measured charge density distribution of ^{208}Pb [FRO87] clearly shows that the region of nearly constant density accounts for a very large fraction (~70 %) of the nuclear volume, thus suggesting that its properties may be largely inferred from those of uniform nuclear matter. The validity of this conjecture is supported by the comparison between the results

of theoretical calculations and the data extracted from the $^{208}\mathrm{Pb}(\mathrm{e},\mathrm{e}'\mathrm{p})^{208}\mathrm{Tl}$ cross sections, measured at NIKHEF back in the 1980s [QUI86]. As shown in Fig. 2-11, the energy dependence of the spectroscopic factors obtained from the experimental analysis turns out to be in remarkably good agreement with that reported in the pioneering work of Ref. [BEN90], in which the deviations from the nuclear matter behavior arising from surface effects were taken into account using a simple phenomenological procedure. The results strongly reinforce the hypothesis that the spectroscopic factors of deeply bound states are mainly determined by short-range correlations, while finite size effects that lead to the appearance of long-range correlations become appreciable in the vicinity of the Fermi surface.

While most existing calculations of the (e, e′K^+) hypernuclear cross-section are based on the mean field approximation underlying the nuclear shell model, the picture emerging from Fig. 2-11 clearly indicates the need of an alternative scheme, allowing for a consistent inclusion of correlation effects. The development of such a scheme would greatly contribute to reduce the systematic error associated with the treatment of the non-strange sector.

In the kinematical regime in which the wavelength associated with the beam particles is small compared to the nucleon-nucleon separation distance in the target, the impulse approximation is expected to be applicable, and the nuclear cross section reduces to the incoherent sum of elementary cross sections involving individual nucleons. Within this scenario, the theoretical calculation of the (e, e′K^+) cross section involves three ingredients: (i) the known cross section of the elementary $\mathrm{ep} \rightarrow \mathrm{e}'\mathrm{K}^+\Lambda$ process, (ii) the spectral function, describing the nucleon momentum and energy distribution in the ^{208}Pb ground state, and (iii) the spectral function containing the information of the bound nucleon. In this context, using a realistic model of the nucleon spectral function, such as the one employed to obtain the results displayed in Fig. 2-11, would greatly reduce the systematic error associated with the treatment of the non-strange sector.

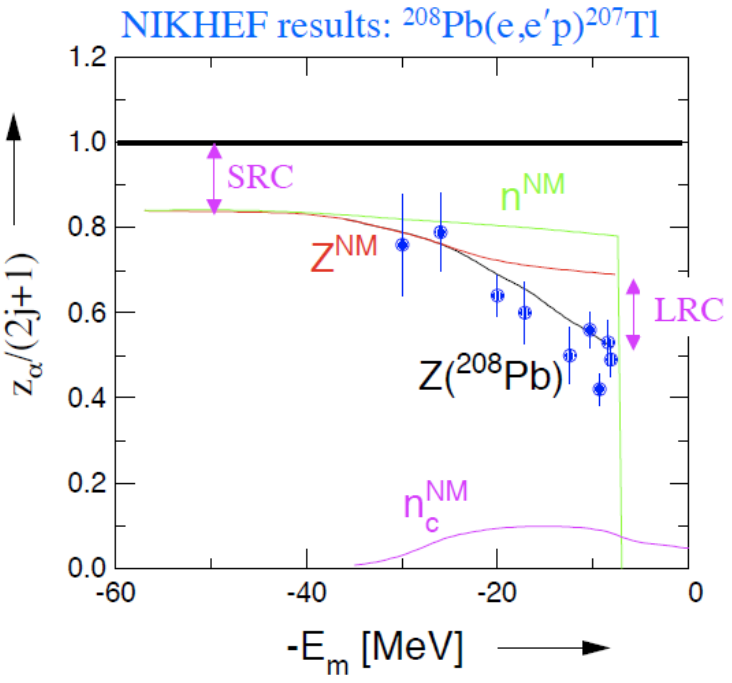

Figure 2-11: Energy dependence of the spectroscopic factors extracted from the measured ^{208}Pb(e, e′p)^{208}Tl cross sections [QUI86], compared to the theoretical resuls [BEN90]. The black and red solid lines, labelled Z(^{208}Pb) and Z^{NM}, correspond to uniform nuclear matter and ^{208}Pb, respectively. The effects of short- (SRC) and long-range-correlations (LRC), the latter arising from surface effects, are indicated.

[AMB60] V. A. Ambartsumyan and G. S. Saakyan, Sov. Astron. AJ 4, 187 (1960).

[THO99] S. E. Thorsett and D. Chakrabarty, Astrophys. J. 512, 288 (1999).

[DEM10] P. B. Demorest, *et al.* , Nature 467, 1081 (2010).

[ANT13] J. Antoniadis, *et al.* , Science 340, 1233232 (2013).

[MIW11] K.Miwa *et al.* , J-PARC E40 experiment.

[PIE08] S. C. Pieper, AIP Conf. Proc. 1011, 143 (2008); Nuovo Cimento Rivista Serie 31, 709 (2008).

[MAR13] P. Maris, J. P. Vary, S. Gandolfi, J. Carlson, and S. C. Pieper, Phys. Rev. C 87, 054318 (2013).

[GAN12] S. Gandolfi, J. Carlson, and S. Reddy, Phys. Rev. C 85, 032801 (2012); S. Gandolfi, J. Carlson, S. Reddy, A. W. Steiner, and R. B. Wiringa, Eur. Phys. J. A 50, 10 (2014).

[FUR09] T.Furumoto, Y.Sakuragi, Y.Yamamoto, Phys. Rev. C 79 (2009) 0011601(R).

[YAM14] Y.Yamamoto, T.Furumoto, N.Yasutake and Th.A.Rijken, Phys. Rev. C 90 (2014) 045805.

[LOR14] D. Lonardoni, F. Pederiva, and S. Gandolfi, Phys. Rev. C 89, 014314 (2014).

[BOD84] A. R. Bodmer, Q. N. Usmani, and J. Carlson, Phys. Rev. C 29, 684 (1984); A. R. Bodmer and Q. N.

Usmani, Phys. Rev. C 31, 1400 (1985).; A. R. Bodmer and Q. N. Usmani, Nucl. Phys. A 477, 621 (1988).

[USM95] A. A. Usmani, S. C. Pieper, and Q. N. Usmani, Phys. Rev. C 51, 2347 (1995); A. A. Usmani, Phys. Rev. C 52, 1773 (1995); Q. N. Usmani and A. R. Bodmer, Phys. Rev. C 60, 055215 (1999); A. A. Usmani and F. C. Khanna, J. Phys. G 35, 025105 (2008).

[IMR14] M. Imran, A. A. Usmani, M. Ikram, Z. Hasan, and F. C. Khanna, J. Phys. G 41, 065101 (2014).

[LON15] D. Lonardoni, A. Lovato, S. Gandolfi, and F. Pederiva, Phys. Rev. Lett. 114, 092301 (2015).

[PIL91] P.Pile *et al.* , *Phys. Rev. Lett.* **66** (1991) 2585.

[HOT01] H. Hotchi, et al. Phys. Rev. C 64, 044302 (2001).

[FRO87] B. Frois and C. N. Papanicolas, Ann. Rev. Nucl. Part. Sci. 37, 133 (1987).

[QUI86] E. N. Quint et al., Phys. Rev. Lett. 56, 186 (1986); E. N. Quint et al., Phys. Rev. Lett. 58, 1727 (1987).

[BEN90] O. Benhar, A. Fabrocini, and S. Fantoni, Phys. Rev. C 41, R24 (1990).

3. Experimental Setup

3.1 Experimental configuration

The proposed experiment is to obtain high precision mass spectroscopy of hypernuclei produced by the (e,e′K^+) reaction and will employ a configuration including a pair of room temperature Septum magnets, the high resolution HRS (Hall A) and the large solid-angle HKS spectrometers, as schematically illustrated in Fig. 3-1.

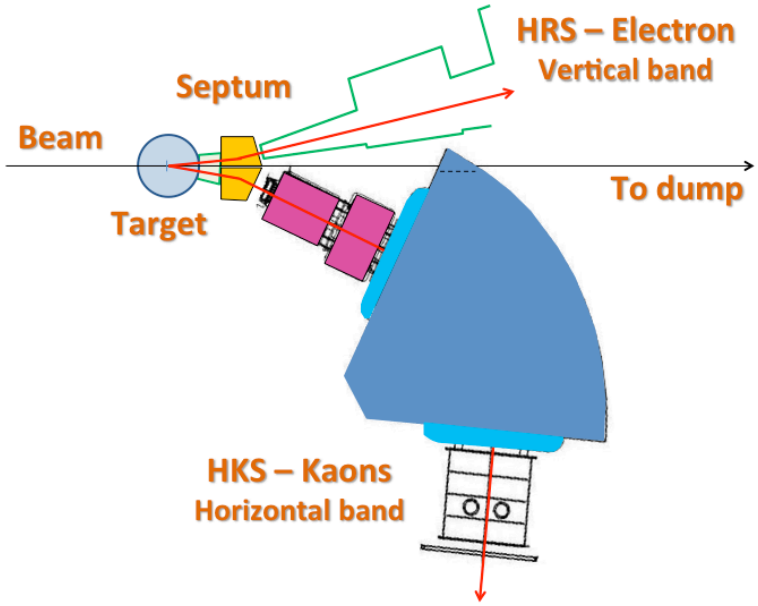

Figure 3-1: Schematic illustration of the experimental layout. A pair of Septum magnets will be used to separate the scattered electrons (analyzed by HRS) and the reaction kaons (analyzed by HKS). All particles at near zero degrees will be sent to the dump.

This pair of Septum magnets will be used to separate the scattered electrons and electro-produced kaons at small forward angles to sufficiently large spectrometer angles, while allowing the post-beam to be directly transported to the dump. It also minimizes the chance for the high rate backgrounds (electrons and positrons) at near zero degrees to enter either of the two spectrometers. The collaboration has demonstrated the technique successful in avoiding the background from e′ and K^+ accidental coincidences by maintaining sufficiently low singles rates at each of the two spectrometers under high luminosity conditions.

One of the Hall A HRS spectrometer will be used to detect and analyze the scattered electrons with a momentum resolution of ~10^{-4} (FWHM) that is crucial to the overall energy resolution for the experiment. With the central scattering plane is defined in the horizontal plane, the vertical bending of HRS provides the important target "Z" vertex reconstruction that will minimize the target "Z" dependence in the optics of the spectrometer system. This is another important feature needed to achieve the ultimate resolution with the extended targets. This is also an important reason for proposing this experiment to run in Hall A.

The HKS spectrometer that was successfully used in the previous Hall C experiments will be used as the kaon spectrometer. It features both a momentum resolution of $\sim 2 \times 10^{-4}$(FWHM) and a large solid angle acceptance that is three times larger than that of HRS. Its application is one of the important factors in achieving both high resolution and high yield in order to study spectroscopy of heavy hypernuclei. Its excellent detector system further cleanly identifies kaons.

One single target chamber will be used for all the planned targets including those to be used for calibrations. The entire system is vacuum connected.

Overall, this experimental design is for (1) the highest possible resolution (~600 keV FWHM in the case of thick solid targets), (2) the highest reachable yield, and (3) the lowest ever achievable background in electro-production of hypernuclei. Both involved spectrometers are well known and used previously with standard detector systems. The only new equipment is the Septum magnets and target system.

3.2 Kinematics

The definition of the kinematics is based on the kinematics using an E = 4.5238 GeV beam, the minimum HRS angle when using a Septum for an e'momentum at ~3 GeV/c, and a maximized overlap of the virtual photon angular range to the HKS angular acceptance for the highest possible production yield. The kinematics parameters and ranges are listed in Table 3-I. The kinematics has a sufficiently large opening angle for both the spectrometers with respect to the beam to avoid the forward scattered electrons and positrons. These were the sources of high accidental background in the previous Hall C hypernuclear experiments.

Table 3-I: Basic kinematics parameters of the Septum+HRS and Septum+HKS systems.

Beam energy (12 GeV mode, 2-passes, injector energy included)	4.5238 GeV
E' (HRS) central angle (horizontal and vertical bites)	7° (±1.5° and ±2.5°)
E' (HRS) central momentum (percentage bite)	3.0296 GeV/c (±4.0%)
Virtual photon central angle ($\phi=\pi$)	14°
Virtual photon energy range	1.37 – 1.62 GeV
Virtual photon momentum range	1.42 – 1.70 GeV/c
Average Q^2	-0.21 $(GeV/c)^2$
K^+ (HKS) central angle (horizontal and vertical bites)	14° (±4.5° and ±2.5°)
K^+ (HKS) central momentum (percentage bite)	1.2 GeV/c (±12.5%)

A GEANT simulation taking into account the realistic and known conditions of both the HRS and HKS was performed. No additional acceptance limitation was included for the new Septum magnets. Fig. 3-2 (a) shows the distribution of the Lab virtual photon angle θ_γ with the kinematics shown in Table I. The shape of the distribution is due to the HRS momentum and angular acceptances. The virtual photons are aiming into the HKS angular acceptance. This maximizes the production yield due to maximized differential cross section. Fig. 3-2 (b) shows the Q^2 range within the acceptance of the system.

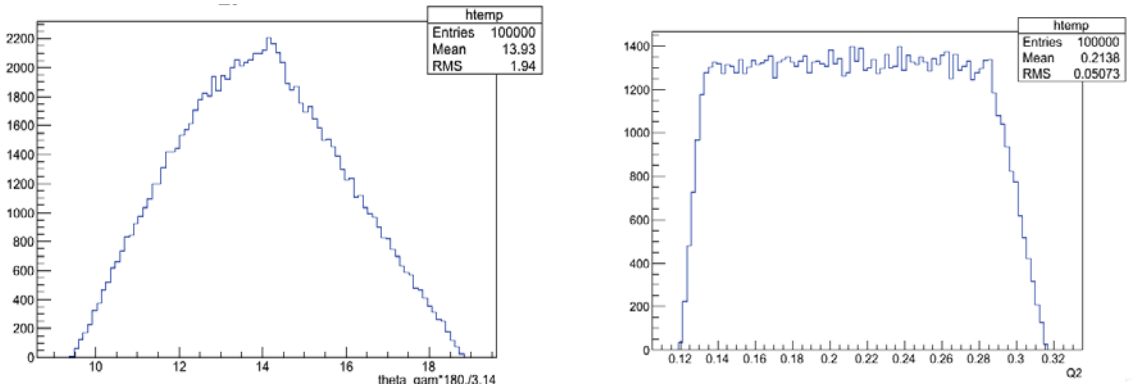

(a) $\theta_{e\gamma}$ Lab (Degrees) (b) Q^2 $(GeV/c)^2$

Figure 3-2: (a) Virtual photon angular distribution (symmetric with respect to $\phi = \pi$ plane defined by the central e and e' plane) in Lab system with respect to beam; (b) Q^2 acceptance.

Fig. 3-3 is an illustration of the e' and K^+ momentum correlation for various mass of hyperons (Λ and Σ^0) and ground state hypernuclei ($^{12}_{\Lambda}B$ and $^{208}_{\Lambda}Tl$). The broadening of Λ and Σ^0 is from the range of recoil angles. Free Λ and Σ^0 productions are important for calibration of the absolute missing mass scale.

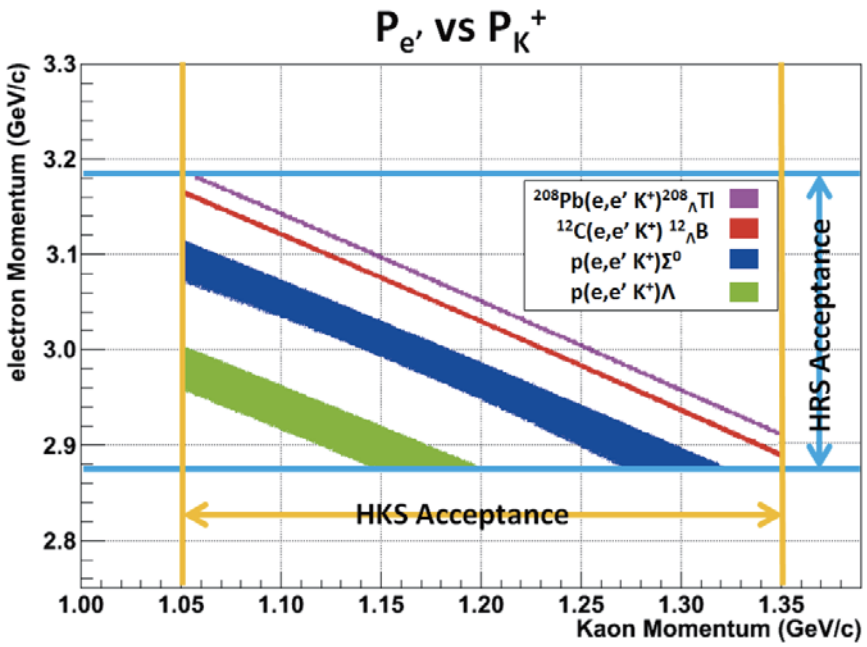

Figure 3-3: Mass correlation in the two dimensional momentum acceptances.

3.3 A draft design of the new Septum magnets

Fig. 3-4 shows the top view of the draft design of the two Septum magnets that will be used in conjunction with the subsequent HRS and HKS spectrometers. The kinematics and optics conditions of the two spectrometers are taken into account. Fig. 3-5 is a 3-D drawing showing the top half of the magnets and their coils. The post beam pipe passes through the half circular opening on the return yoke. This section of pipe uses magnetic field shielding material to minimize the influence from the fringe field on the exiting beam. Small correctors can be mounted behind the Septum to aim the beam correctly at the hall dump. Both the Septum technique and application of correctors were successfully used in the previous experiments.

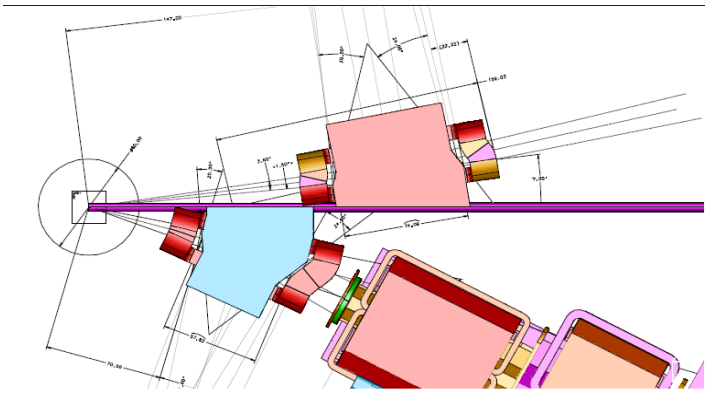

Figure 3-4: Illustration of the draft design of the two Septum magnets and their geometric relationship to the target chamber and subsequent spectrometers.

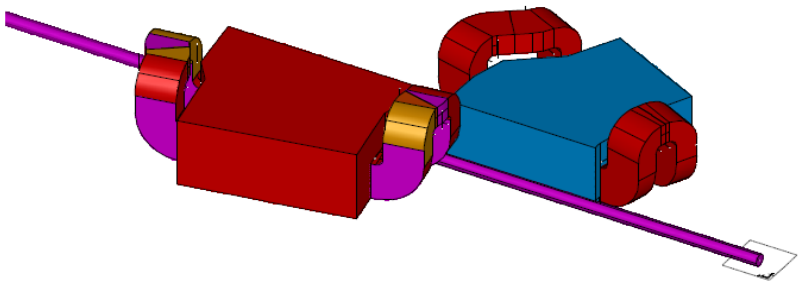

Figure 3-5: 3-D illustration of the two Septum magnets and the post beam pipe. Minimum influence of the fringe field to the post beam will be achieved by making the Septum "H" type and using magnetic shielding material for this section of pipe. Small correctors will be needed behind the Septum.

The major design parameters for consideration are listed in Table 3-II. The front distance is minimized to keep the HKS total path length as short as possible to maximize the K^+ survival rate. At the same time, sufficient space is maintained for the target chamber.

A common sieve slit device may be mounted inside the target chamber where no fringe field from Septum is present. Introduction of the incline angles α and β is to reduce the horizontal dispersion and minimize the influence to the horizontal angular acceptance. The central and bend angles are driven by the conditions for separation of the forward scattered particles, the required minimum space between the two spectrometers, and maximization of the yield. The field strength is chosen to be as low as possible to simplify the magnet design. The gaps are decided based on the vertical acceptance requirement from the HRS and HKS spectrometers.

Table 3-II: Basic design parameters of the Septum magnets for the HRS and HKS spectrometers.

Basic parameters	Septum (HRS)	Septum (HKS)
Front drift distance	147 cm	70 cm
Central angle	7°	14°
Horizontal angular bite	~±1.5°	~±4.5°
EFB incline angle α	-20°	-20°
EFB incline angle β	-24°	-24°
Bending angle ϕ	7°	12°
Field B	1.45 T	1.45 T
Rotation radius	707.49 cm	276.05 cm
Path length	86.44 cm	57.82 cm
Total integral Bdl	1.2534 T*m	0.8384 T*m
Gap	18 cm	12 cm

The target point will be determined by the Septum+HRS system. The Septum+HKS system is then located accordingly. The common target chamber has an outside dimension of 60-90 cm diameter. The target ladder contains both liquid/gas target cells and solid targets determined by the physics program and calibration needs. The ladder should be cooled to allow usage of the highest possible beam current. The chamber will have one incoming beam line connection port and exiting connection ports to the two spectrometers and the beam dump line. The sieve slit/collimator plates can be mounted on the target chamber and surveyed with respect to the target coordinates.

3.4 Yield rate comparison to the previous experiments

The new configuration of Septum+HRS/Septum+HKS aims to obtain almost background free spectroscopy for hypernuclei below the medium heavy mass region while maintaining good signal/accidental ratio for the heavy mass region.

The ground state peak of the $^{12}_{\Lambda}$B hypernucleus contains two states, $J^p = 1^-$ and 2^-. The combined photo-production cross-section with E_γ of about 1.5 GeV and θ_γ near zero is well known to be about 100 nb/sr in good agreement with both theory and (Hall A and C) experiments. Thus, the measured production yield of this peak by the Hall A and C experiments can be used to estimate the predicted yield with the new configuration. Table 3-III lists the gain factors over the previous Hall A and C experiments for various contributions, the combined total gain factor, and the estimated yield rate from known cross sections or production rates using the same luminosity. The results based on the previous experiments in Hall A and Hall C are consistent and their average is about 0.55 counts/hr/(1.0 nb/sr). A GEANT simulation using more precise information about the HKS and HRS predicted similar yield rates, 0.54 counts/hr/(1.0 nb/sr).

Table 3-III: Gain factor over the previous experiments and estimated production rate using the same luminosity.

Itemized gain factors by the new configuration	Over the previous Hall A experiment	Over the previous Hall C experiment
Integrated virtual photon flux ($\int\Gamma(E,E',\theta)dE'd\Omega$) per electron	2.16	0.91
K^+ survival rate	1.86	0.93
Integrated photo-production cross section ($\Delta\Omega_K$)	1.35	0.66
Beam current: 100μA	1	1
C target thickness: 100mg/cm^2	1	1
Total gain factor	5.42	0.56
Experimentally measured count rate (scaled to the same lum.)	10 counts/hr	100 counts/hr
Estimated count rate ($^{12}_{\Lambda}$B gs(1^- , 2^-), per 100nb/sr)	54 counts/hr	56 counts/hr

Although the yield rate is about half of the previous Hall C experiment which emphasized the yield, the production yield is still sufficiently high. The most important feature of the

new configuration is the low accidental background. This is a significant difference from the previous Hall C experiments. In other words, the new configuration can be considered a significant upgrade of the Hall A experiment and increases its physics yield rate by a factor of five.

3.5 Spectrometer calibrations

Calibration of the spectrometer system is extremely important for the experiment to achieve its goal of high precision in determining the absolute mass (or Λ binding energy) and mass resolution. Standardized calibration methods and procedures successfully developed in the previous experiments will be applied again. A significant advantage of the new configuration is that these methods and procedures become more straight forward and can further improve the precision with much less analysis effort. This is because the two spectrometers are almost optically decoupled and there will be less information entanglement in the calibration data.

Some of light solid targets will be used for calibration as well as for precise determination of B_Λ. From experiences of previous hypernuclear programs at JLab, we learned that data for various solid targets with different energy loss contributions are quite useful to tune the backward matrix. We are considering using well studied CH_2, ^{10,11}B, ^{6,7}Li, ^{12}C targets for this purpose.

In addition to the above standard calibrations developed mainly for thin solid targets in the past, new calibrations will be needed for the extended target to futher ensure excellent energy resolution. The major additional calibration is the reconstruction of the reaction ΔZ. A sequence of carbon foils at different Z will be used to collect data with known reaction Z position. ΔZ will be fit as a function of the 8 measured focal plane parameters from both spectrometers. For extended target, the ΔZ correction will be used in the momentum and reaction angle reconstructions.

Both thin CH_2 and extended gaseous H_2 targets will be used as part of overall calibration. Simultaneous production of Λ and Σ^0 particles from CH_2 is important in calibrating the precise absolute mass scale while their production from the (extended) H_2 target will be an important optimization of the ΔZ dependence in the reconstructions.

3.6 Conclusion of this section

The configuration designed for the future hypernuclear physics experiments promotes high yield and clean spectroscopy. It makes possible the study of hypernuclei with high precision in a wide mass range (from few-body with extended targets to heavy systems with thin solid targets) at small Q^2 and a significant range of CM $\theta_{\gamma K}$ angles.

4. Yield, resolution estimation and requested beamtime

The experiment will use two types of targets: 1) gas cryogenic targets and 2) solid targets. Detailed design of the gaseous cryogenic targets will be optimized in collaboration with the JLab target group. For now, we assumed a cylinder cell of 20 cm length, 200 psi (13.6 atm) for gas targets and 100 mg/cm^2 foils for solid target (500 mg/cm^2 for CH_2).

The estimation was carried out with the well-established GEANT4 model for HKS and a newly modeled HRS with an index dipole magnetic field calculated by TOSCA.

4.1 Expected mass resolution

The following factors contribute to the total mass resolution of the (e,e'K$^+$) experiment and they are summarized in Table 4-I.

1. Spectrometers' momentum resolution.

   Since HKS (K$^+$) and HRS (e') are already established spectrometers, relative momentum resolutions are known.

2. Beam energy resolution.

   We assumed $dE/E < 5 \times 10^{-5}$ for a 4.5 GeV electron beam.

3. Kinematic broadening due to uncertainty of the K$^+$ and e' scattering angles.

   The uncertainties of the K$^+$ and e' emission angles originate from multiple scattering through the materials between the target and tracking chambers in addition to the angular resolution of the spectrometer itself. This effect is significant for hyperon elementary production or light hypernuclei, but less significant for heavier nuclei since the recoil of the hypernuclei is much smaller.

4. Energy loss and straggling in the target.

   Since our vertex resolution is not enough to determine the reaction point in the solid target (typically the thickness is less than a half mm while the gaseous target thickness is 200 mm), so energy loss of charged particles can be corrected only as an average. Its distribution including straggling will contribute the final mass resolution. For kaons, both the energy loss distribution due to the reaction point distribution and straggling will contribute while the sum of energy losses in the target for the beam and scattered electron is roughly constant and thus only straggling is problem. These effects were estimated with a GEANT simulation.

5. Uncertainty of the reaction point in the beam axis direction (ΔZ).

As mentioned already, only the HRS has sensitivity to the reaction point in the Z direction, meaning that the HKS does not have it to first order since both the Septum and HKS are horizontal bending magnets. Uncertainty in Z does not make a problem for solid targets since their thickness is typically less than 0.5 mm, however, it affects the resolution for gaseous targets. Using a GEANT simulation, ΔZ resolution was estimated for the HRS and the reaction points in the simulation for the HKS were randomly distributed in ΔZ to estimate the deterioration of the HKS resolution. In the real analysis, the focal plane information of HRS and HKS can simultaneously be used to reach the best resolution.

Table 4-I: Estimation of mass resolution for selected targets (unit is in keV).

Target	Gas ^{1}H (30 mg/cm^2)	Gas ^{3}H (89 mg/cm^2)	Gas ^{4}He (58 mg/cm^2)	^{12}C (100 mg/cm^2)	^{40}Ca (100 mg/cm^2)	^{208}Pb (100 mg/cm^2)
Beam	220	220	220	220	220	220
e' spectrometer	600	555	560	300	300	300
K spectrometer	240	220	220	220	220	220
K, e' angles	2500	940	250	105	35	10
Energy loss/straggling	230	230	220	380	330	340
Total	2600	1160	720	590	550	550

4.2 Expected yield and required beamtime

Using the estimated $^{12}_{\Lambda}B_{g.s.}$ yield rate in section 3.4, hypernuclear yields for various targets are summarized in Table 4-II.

It was assumed that the background originates from the accidental coincidence between K^+ and e' and the background spreads uniformly in the acceptance of the missing mass. The quasi-free production cross section of K^+ and e' are in proportion respectively to $A^{0.8}$ which was estimated from the $^{12}C(\gamma,K^+)$ reaction and A which is expected in DIS region. All solid targets' thicknesses are normalized to be 100 mg/cm^2 except for CH_2.

Necessary beamtime was estimated to have enough events for major shell peak energies to be statistically determined with an accuracy of 50 keV. Signal to noise ratio is calculated with the numbers of signal in $\pm 1\sigma$ of Gaussian peak and background events under the peak.

Table 4-II: Yields estimation for various targets.

Target and objective hypernucleus	Beam current (μA)	Target thickness (mg/cm^2)	Assumed cross section (nb/sr)	Expected Yield (/hour)	Num. of events	Req. beamtime (hours)	B.G. Rate (/MeV/h)	S/N ($\pm 1\sigma$)	Comments
CH_2	2	500	200	19	1000	54	0.05	252	Calibration
^{6,7}Li	50	100	10	5.4	150	28	1.3	4.9	Calibration
^{9}Be	100	100	10	36	150	9	4.7	8.8	Calibration
^{10,11}B	25	100	10	16	150	19	0.29	33	Calibration
^{12}C	100	100	100	54	2000	37	4.4	17	Calibration
Subtotal for calibration targets						**147**			
H_2 (Λ, Σ^0)	20	30	200	78	4000	52	0.09	1.3	Gas Calibration
D_2 ([nΛ])	20	59	1	0.38	50	130	0.09	1.3	Gas
T_2 ([nnΛ])	20	89	1	0.38	50	130	0.18	1.4	Gas
^{3}He ($^{3}_{\Lambda}$H)	20	58	5	1.3	100	80	0.08	18	Gas, Reference
^{4}He ($^{4}_{\Lambda}$H)	20	58	20	3.8	1000	266	0.07	57	Gas
Subtotal for cryogenic targets						**658**			
^{40}Ca ($^{40}_{\Lambda}$K)	50	100	20	1.6	200	124	0.86	2.7	
^{48}Ca ($^{48}_{\Lambda}$K)	50	100	20	1.4	200	148	0.84	2.4	
^{208}Pb($^{208}_{\Lambda}$Tl)	25	100	10	0.16	s_Λ 50 p_Λ 200	642	0.16	0.7 2.8	
Subtotal for heavier targets						**914**			
Total						**1719**			

5. Summary

Based on more than a decade of experience at JLab, Hall A and Hall C, the JLab Hypernuclear Collaboration proposes the following experiment to investigate the ΛN interaction:

1. The study of elementary Λ electro-production, charge symmetry breaking effects of the ΛN interaction, and the search for exotic chargeless hypernuclei with gaseous light targets,

   and

2. Precise B_Λ measurement for medium to heavy hypernuclei.

The experiment will utilize well-established magnetic spectrometers HRS and HKS that were successfully used in the previous hypernuclear programs in Hall A and Hall C.

Here, we summarize the important parameters and required resources for conducting of the experiment.

Key Experimental Parameters:

Beam energy: 12 GeV mode, 2-pass: 4.5238 GeV, Hall-A,

Requested beam time in total: 1730 h = 72 days.

Range of beam currents: 2 to 100 μA,

Major apparatus: HKS, HRS, and Septa magnets.

Required resources:

Major installations and new support structures:

HKS and Septa need major installation of magnets and detector packages.

HKS needs a new support for Hall A.

New support structure for the Septa and Shielding houses for detectors are necessary.

Major Equipment

Magnets: HRS in Hall A, HKS (KQ1, KQ2 and KD), new Septum magnets (the 2nd can be the previously used super-conducting septum)

Power Supplies: HKS-D (252V, 1254A), HES-D (250V, 1100A) have own PS's provided by Tohoku University, all other PS's necessary are to be prepared by JLab.

Targets: Cryogenic target system for gaseous H_2 , D_2 , T_2, ^{3}He and ^{4}He.

Solid targets: CH_2, ^{6,7}Li, ^{9}Be, ^{10,11}B, ^{12}C, ^{40}Ca, ^{48}Ca, ^{208}Pb.

Detectors: Standard detectors for HRS,

HKS-detector package (Drift Chambers, TOF walls, Aerogel Chrenkov, Water Cherenkov)

Electronics: Standard electronics, F1-TDCs, Amp-discriminator cards for drift chambers, FPGA based special trigger modules developed by Tohoku University (TUL-8040)

Computer Hardware: Standard

Possible Hazard

Cryogenics: Standard cryotarget in Hall-A

Electrical Equip.: high voltages for PMT, Drift Chambers, large currents for magnets

Flammable gas for drift chambers: Argon Ethane 50/50, 0.15 l/min each for HRS and HKS.

Targets: Condition 1,2 are single spectrometer calibration with elastic scattering. Condition 3-7 are for calibration with coincidence measurement, 8-12 are for the physics run with gaseous cryogenic target and 13-15 with solid medium and heavy targets.

Condition #	Beam Energy (MeV)	Beam Current (μA)	Special Request	Target Material	Material Thickness (mg/cm^2)	Est. Beam on time (hours)
1	1200	10		Ta	100	10
2	3000	10		Ta	100	10
Single Arm. Calib						**20**
3	4523.8	2	2×2 mm^2 raster	CH_2	500	54
4	4523.8	50	2×2 mm^2 raster	Li	100	28
5	4523.8	100	No raster	^{9}Be	100	9
6	4523.8	25	2×2 mm^2 raster	B	100	19
7	4523.8	100	No raster	^{12}C	100	37
Subtotal calibration						**147**
8	4523.8	20	Gas	H_2	30	52
9	4523.8	20	Gas	D_2	59	130
10	4523.8	20	Gas	T_2	89	130
11	4523.8	20	Gas	^{3}He	58	80
12	4523.8	20	Gas	^{4}He	58	266
Subtotal gas targets						**658**
13	4523.8	50		^{40}Ca	100	124
14	4523.8	50		^{48}Ca	100	148
15	4523.8	25	2×2 mm^2 raster	^{208}Pb	100	642
Subtotal heavy targets						**914**
Grand Total						**1739**

Appendices

A. Electro-magnetic background in the kaon spectrometer

The HKS suffered from high rate backgrounds during the E05-115 runs. The source of background was carefully analyzed and a detailed GEANT4 simulation revealed the source of it.

The HKS with a Splitter magnet used in E05-115 was designed to avoid secondary e^+'s created in the target with its' optics. Such e^+ cannot reach the HKS detectors, however, some of them will hit the material just outside of the HKS dipole and create tertiary e^+ e^- pairs. Though such a probability is small, the large-Z target created lots of secondary e^+'s and then the tertiary e^+e^- background was not negligible.

Simulation with the GEANT4 model which includes vacuum extensions shows the source position of such background (Fig. A-1). The tracking information of real data proved that the majority of the background originated from a flange for a NMR port on the vacuum extension box.

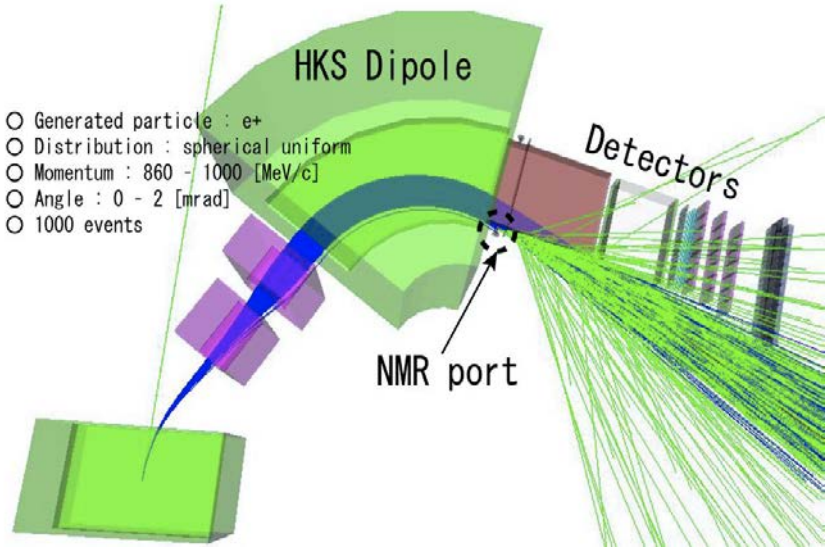

Figure A-1: GEANT4 simulation for electro-magnetic background experienced in the E05-115 experiment.

We modeled a septum magnet and combined it with the well-established HKS model in GEANT4. In the simulation of Septum + HKS, 10^{10} electrons were introduced in 100 mg/cm^2 Pb target and no secondary e^+'s reached the HKS exit.

It corresponds to 16 μs of 100 μA beam irradiation and thus background in the HKS originating from this source should be less than 62.5 kHz which does not cause any serious problem to the HKS detectors.

B. Theoretical predicted spectroscopy for selected hypernuclei

There are theoretical predictions on expected missing mass spectra to be obtained by the (e, e′K^+) reactions. This information was used in the design of the proposed experiment and will be further used in the detailed analysis to extract hypernuclear structure information.

B.1 ^{4}He(e, e′K^+)$^4_\Lambda$H reaction

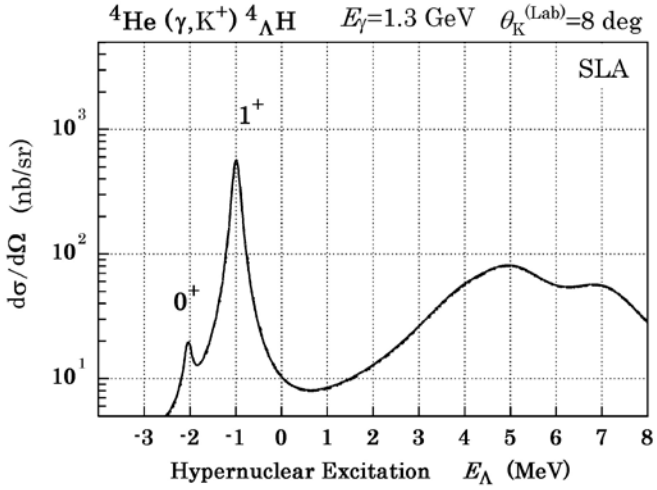

Figure B-1: Expected cross section for the ^{4}He(e, e′K^+)$^4_\Lambda$H reaction [MOT14].

Figure B-1 shows the expected cross section for the ^{4}He(e, e′K^+)$^4_\Lambda$H reaction calculated with the distorted wave impulse approximation (DWIA) [MOT14] assuming the elementary amplitude of an isobar model, Saclay Lyon A (SLA) [DAV96].

It is very sensitive to the elementary process, p(e,e'K^+)Λ, to be measured by the proposed experiment. The absolute cross section may have some uncertainty, however, the tendency for the 1^+ cross section to be much larger than the ground state (0^+) cross section at forward angles is essentially model-independent. Therefore in the kinematics of the proposed experiment, what we will see in the missing mass spectrum of ^{4}He(e,e'K^+)$^4_\Lambda$H is mostly the 1^+ peak in the bound region which is the missing information for the discussion of the CSB of A=4 hypernuclear systems.

[DAV96] J.C. David, C. Fayard, G.-H. Lamot, B. Saghai, **Phys. Rev. C 53**, 2613 (1996);
T. Mizutani, C. Fayard, G.-H. Lamot, B. Saghai, **Phys. Rev. C 58**, 75 (1998).
[MOT14] T. Motoba, private communication.

B.2 ^{40}Ca(e,e'K$^+$)$^{40}_{\Lambda}$K reaction

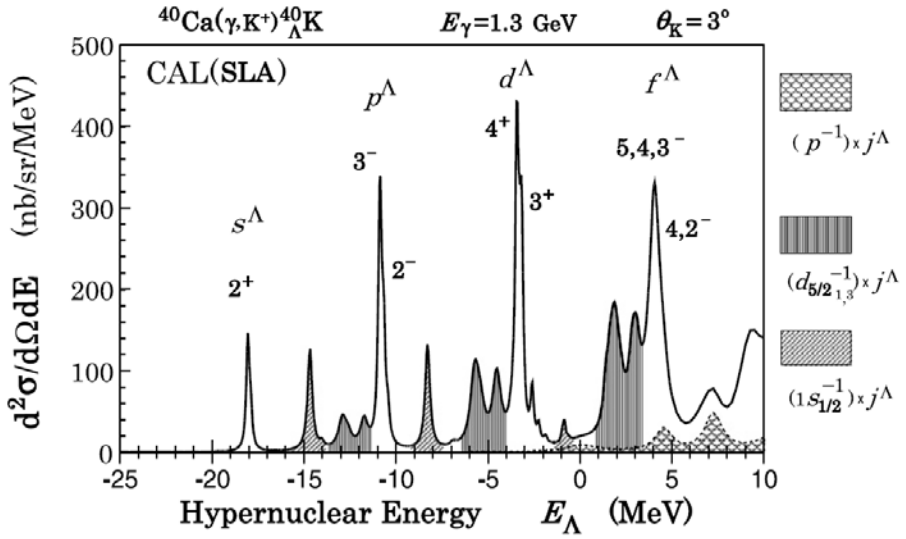

Figure B-2: Calculated ^{40}Ca(γ,K$^+$)$^{40}_{\Lambda}$K excitation function by DWIA with SLA model. The calculation assumed E_γ = 1.3 GeV, $\theta_{\gamma K}$ = 3° and function *ls*-splitting of 0.17(2*l* +1) MeV [BYD12].

The ^{40}Ca target is doubly *LS*-closed up to the $0d_{3/2}$ shell. As shown in Figure B-2, the ^{40}Ca(γ,K$^+$)$^{40}_{\Lambda}$K excitation function calculated by DWIA with the SLA model [Byd12], the $^{40}_{\Lambda}$K's natural parity states (2^+,3^-,4^+) are expected to be populated predominantly. Therefore, we can extract $s^{\Lambda}_{1/2}$, $p^{\Lambda}_{3/2}$ and $d^{\Lambda}_{5/2}$ energies from these peaks with less ambiguity. We can expect major shell peaks (Λ in s, p, d, f waves) with the production cross section of 100 nb/sr and core excited states with 10-100 nb/sr.

[BYD12] P. Bydžovský and D. Skoupil, **arXiv:1212.0337v1** [nucl-th].

B.3 ^{208}Pb(e,e'K$^+$)$^{208}_{\Lambda}$Tl reaction

Figure B-3 shows the ^{207}Tl core nucleus level scheme. Table B-I shows the spectroscopic factors measured in ^{208}Pb(d,^{3}He)^{207}Tl reaction. They are large enough for many low-lying states of ^{207}Tl core nucleus (up to excitation energy ~4 MeV) and that the corresponding hypernuclear states with a Λ coupled to these core states are populated.

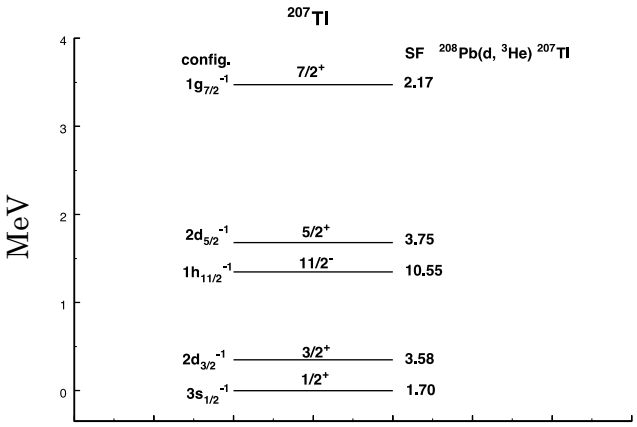

Figure B-3: ^{207}Tl core nucleus level scheme.

Table B-I: ^{207}Tl energy spectrum, dominant configurations and spectroscopic factors.

E_x MeV	J^π	Config.	C^2S
0.000	1/2+	$2s^{-1}_{1/2}$	1.70
0.351	3/2+	$1d^{-1}_{3/2}$	3.58
1.348	11/2−	$0h^{-1}_{11/2}$	10.6
1.683	5/2+	$1d^{-1}_{5/2}$	3.75
—	—	—	—
3.747	7/2+	$0g^{-1}_{7/2}$	2.17

Figure B-4 shows the spectrum for ^{208}Pb(γ,K$^+$)$^{208}_{\Lambda}$Tl calculated for our kinematics using the Saclay Lyon A elementary amplitudes with assumed resolution of 500 keV (FWHM). The Λ is assumed to be weakly coupled to the proton-hole states of ^{207}Tl, which is strongly populated in (e,e'p) or (d,3He) reactions on ^{208}Pb. The Λ single-particle energies were calculated from a Woods-Saxon well fitted to energies derived from the ^{208}Pb(π^+,K$^+$)$^{208}_{\Lambda}$Pb reaction. States based on the closely-spaced p 2s1/2^{-1} and p 1d3/2^{-1} states are represented by blue bars and curves. Likewise for the p 0h11/2^{-1} and p 1d5/2^{-1} states shown by red bars and curves. The successive blue and red peaks correspond to the population of the s, p, d, f, g, and h Λ's orbits. The green lines correspond to the noded 1s, 1p, 1d/2s, and 1f Λ orbits. The remaining (wiggly) curves correspond to strength based on deeper and fragmented proton-hole strength.

The expected spectrum shown in Figure B-4 can be compared with the only available A=208 hypernuclear data from ^{208}Pb(π^+, K$^+$)$^{208}_{\Lambda}$Pb.

[MIL13] D.J.Millener and T.Motoba, private communication (2013).
[HAS96] T.Hasegawa *et al.*, *Phys Rev.* **C 53** (1996) 1210.

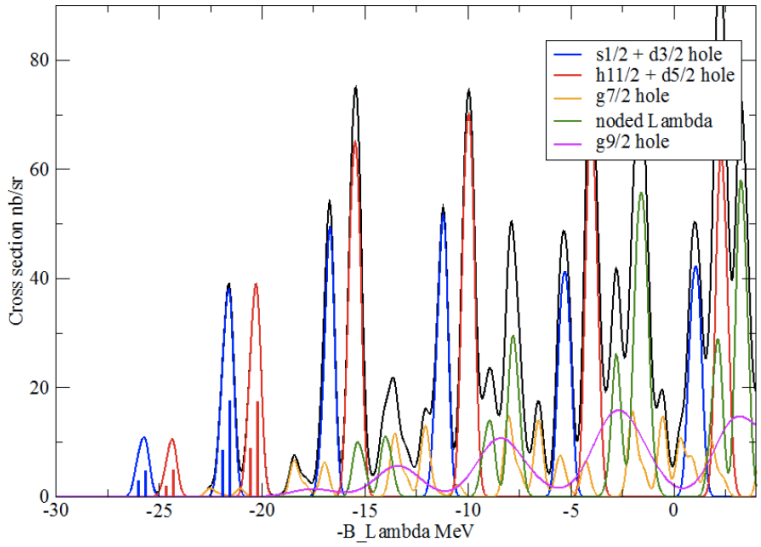

Figure B-4: Expected $^{208}\mathrm{Pb}(e,e'K^+)^{208}_{\Lambda}\mathrm{Tl}$ excitation energy plot [MIL13].

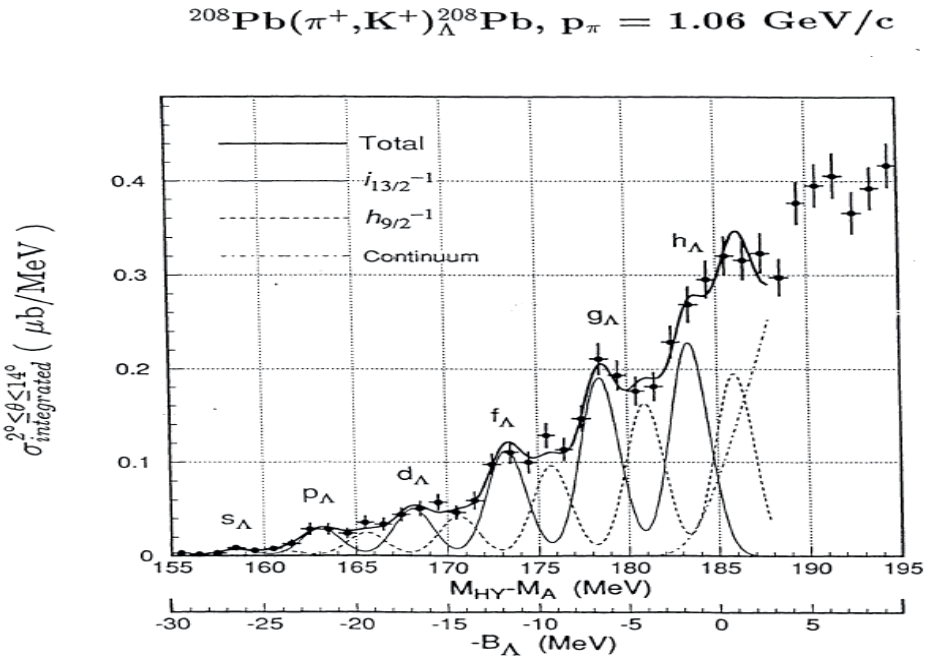

Figure B-5: Experimental $^{208}\mathrm{Pb}(\pi^+,K^+)^{208}_{\Lambda}\mathrm{Pb}$ excitation energy plot [HAS96].